A Damped Subspace Splitting Algorithm for Constrained Density Functional Theory*

Yuanming Su[1], Yukuan Hu[2], Xin Liu[1], and Guanghui Hu[3]

[1]State Key Laboratory of Mathematical Sciences, Academy of Mathematics and Systems Science, Chinese Academy of Sciences, Beijing 100190, China and School of Mathematical Sciences, University of Chinese Academy of Sciences, Beijing 100049, China

[2]CERMICS, CNRS, École des Ponts, Institut Polytechnique de Paris, 6-8 avenue Blaise Pascal, Cité Descartes, 77455 Marne-la-Vallée, France

[3]State Key Laboratory of Internet of Things for Smart City and Department of Mathematics, University of Macau, Macao, China

arXiv:2608.05682v1 [math.OC] 6 Aug 2026

August 7, 2026

Abstract

Constrained density functional theory (CDFT) provides a powerful framework for describing electronically excited and charge-localized states, which underlie a broad range of physical and chemical phenomena. However, the discretized optimization problems arising from CDFT calculations remain challenging, owing to the presence of both the Stiefel manifold constraint and additional nonconvex quadratic constraints. Existing algorithms either fail to enforce the quadratic constraints with high accuracy or face convergence issues due to double-loop iterative structures. In this paper, we first derive a subspace-splitting reformulation that decouples the two groups of constraints, by exploiting the inherent rotation invariance and introducing a nonlinear subspace alignment constraint. Based on this reformulation, we propose a single-loop damped alternating direction method of multipliers, called DASSP. To the best of our knowledge, DASSP is the first algorithm for CDFT calculations with rigorous convergence guarantees. Each iteration of DASSP comprises a spectral minimization step, a projected gradient step, and a damped dual ascent step, all of which admit efficient implementations. Numerical results on synthetic and realistic CDFT problems demonstrate that DASSP attains high feasibility accuracy and exhibits favorable efficiency without compromising robustness. We expect that this work will pave the way toward reliable and efficient large-scale CDFT applications.

1 Introduction

Building on the seminal works of the 1960s [31, 35], density functional theory (DFT) has been the workhorse for first-principles simulations of ground-state properties of molecules, materials, and nanosystems [9]. While the ground states are recognized to be the most stable in nature, excited states play a crucial role in a wide range of physical and chemical processes and are

*The work of Xin Liu was supported in part by the National Natural Science Foundation of China (No. 12125108). The work of Yukuan Hu has received funding from the European Research Council (ERC) under the European Union's Horizon 2020 research and innovation program (grant agreement EMC2 No. 810367). The work of Guanghui Hu was supported by The Science and Technology Development Fund, Macao SAR (Nos. 0068/2024/RIA1, 001/2024/SKL), National Natural Science Foundation of China (No. 11922120), MYRG of University of Macau (No. MYRG-CRG2024-00042-FST).

essential for understanding phenomena such as light absorption, emission, and energy transfer [5, 56]. To describe electronically excited or charge-localized states within the DFT framework, several extensions and approaches have been developed, including constrained DFT (CDFT) [14, 34].

This paper is concerned with the optimization problems arising from CDFT, which have received little attention from the mathematics community, in stark contrast to the DFT [11, 44]. In its general form [23, 34], for an N-electron system, the CDFT problem amounts to solving[1]

$$\begin{aligned} \inf_{\{\boldsymbol{\psi}_i\}_{i=1}^N} \quad & E[\boldsymbol{\rho}[\{\boldsymbol{\psi}_i\}_{i=1}^N]], \\ \text{s. t.} \quad & \int_{\mathbb{R}^3} \boldsymbol{\psi}_i^\top(\boldsymbol{r})\boldsymbol{\psi}_j(\boldsymbol{r})\,\mathrm{d}\boldsymbol{r} = \delta_{ij}, \quad i,j = 1,\dots,N, \\ & \sum_{\sigma,\sigma'\in\{\uparrow,\downarrow\}} \int_{\mathbb{R}^3} w_j^{\sigma,\sigma'} \rho^{\sigma,\sigma'}[\{\boldsymbol{\psi}_i\}_{i=1}^N](\boldsymbol{r})\,\mathrm{d}\boldsymbol{r} = N_j, \quad j = 1,\dots,m. \end{aligned} \tag{1.1}$$

Here, $\{\boldsymbol{\psi}_i := (\psi_i^\uparrow, \psi_i^\downarrow)^\top\}_{i=1}^N$ denote a set of orthonormal spinor orbitals, with $\psi_i^\uparrow$ and $\psi_i^\downarrow$ the spin-up and spin-down components, respectively; $\boldsymbol{\rho} := \left[\begin{smallmatrix} \rho^{\uparrow,\uparrow} & \rho^{\uparrow,\downarrow} \\ \rho^{\downarrow,\uparrow} & \rho^{\downarrow,\downarrow} \end{smallmatrix}\right]$ refers to the spin-density matrix, defined by $\boldsymbol{\rho} = \sum_{i=1}^N \boldsymbol{\psi}_i\boldsymbol{\psi}_i^\top$; E represents the Kohn-Sham energy functional in $\boldsymbol{\rho}$ [35][2]; $\{w_j^{\sigma,\sigma'}\}_{\sigma,\sigma'}$ are the weight functions associated with the j-th constraint and $N_j \in \mathbb{R}$ $(j = 1,\dots,m)$. Such a formulation encompasses several practical situations [23, 34]. For example, to constrain the charge of a spatial fragment, one may choose the weight functions such that $w_j^{\uparrow,\uparrow} = w_j^{\downarrow,\downarrow} = w_j$ and $w_j^{\uparrow,\downarrow} = w_j^{\downarrow,\uparrow} \equiv 0$, where w_j is a smoothed indicator function of the fragment. This yields a constraint on the local charge density, useful for characterizing charge-transfer states [61, 62]. In noncollinear DFT, it is common to constrain local atomic magnetic moments in order to investigate energy landscapes of magnetic materials and to construct machine-learned surrogates [48, 64, 65, 67]. This can be achieved by defining the weight functions using Pauli matrices and smoothed indicator functions localized around atoms. In these typical applications, m is at most on the order of $\mathcal{O}(N_{\mathrm{nuc}})$, with $N_{\mathrm{nuc}} \in \mathbb{N}$ the number of nuclei. We also note that the CDFT reduces to the DFT when m equals zero.

The continuous formulation (1.1) can be discretized upon choosing suitable basis sets; interested readers are referred to Appendix A. The resulting optimization problem is of the form

$$\min_X \ f(XX^\top), \quad \text{s. t. } X \in \mathrm{St}_p(\mathbb{R}^n), \ \mathrm{Tr}(X^\top W_j X) = b_j, \quad j = 1,\dots,m, \tag{1.2}$$

which involves the Stiefel manifold $\mathrm{St}_p(\mathbb{R}^n) := \{X \in \mathbb{R}^{n\times p} : X^\top X = I_p\}$ together with m additional nonconvex quadratic constraints defined by $W_j \in \mathbb{S}^n$ and $b_j \in \mathbb{R}$ $(j = 1,\dots,m)$. For simplicity, we impose the following blanket assumption.

Assumption 1.1 (Blanket assumption)**.**

(A1) *Problem (1.2) has at least one feasible point.*

(A2) *The (Riemannian) linear independence constraint qualification is fulfilled at any local minimizer X of problem (1.2), namely, $\{(I_n - XX^\top)W_jX\}_{j=1}^m$ are linearly independent.*

Remark 1.1. Assumption 1.1 (A2) implies the necessity of the Karush-Kuhn-Tucker (KKT) stationary conditions for any local minimizer of problem (1.2) [6].

[1] We consider real Hamiltonians without spin-orbit coupling or magnetic fields; therefore, the spinor orbitals can be assumed to be real-valued.

[2] We consider the energy functional in density, allowing the use of all local and semi-local as well as some non-local exchange-correlation functionals. See the perspective [9] for more details.

In the context of CDFT, the matrix X, the objective function f, and the matrices $\{W_j\}_{j=1}^m$ are derived from the discretizations of spinor orbitals, energy functional, and weight functions, respectively. From the optimization point of view, the main difficulty in solving problem (1.2) lies in the coupling of manifold constraints with additional quadratic constraints. If the latter are missing, problem (1.2) becomes an optimization problem on the Stiefel manifold and a wide range of optimization algorithms are applicable; see [1, 32] and the references therein. One could also perform the self-consistent field (SCF) fixed-point iteration, which is a conventional option in DFT calculations [11, 44]. The presence of quadratic constraints spoils such geometrical structure.

There are mainly two classes of methods for solving problem (1.2) in the CDFT community. The most straightforward one gets rid of the m quadratic constraints by adding penalty terms to the objective function [48]. With a fixed penalty parameter $\sigma > 0$, the quadratic penalty problem, for instance,

$$\min_X \ f(XX^\top) + \sigma \sum_{j=1}^m \Big(\mathrm{Tr}(X^\top W_j X) - b_j\Big)^2, \quad \text{s. t.} \quad X \in \mathrm{St}_p(\mathbb{R}^n) \tag{1.3}$$

could be solved by either optimization algorithms on the Stiefel manifold or by the SCF iteration mentioned above [1, 11, 32, 44]. Such a methodology has been implemented by materials simulation software packages such as VASP [39, 40]. However, since the exactness of penalty is not guaranteed[3], one needs to choose a large penalty parameter to reduce the feasibility violation, while an excessively large penalty parameter can lead to numerical instability.

The second class consists of double-loop methods that achieve feasibility by solving a sequence of simpler subproblems at each iteration [10, 23, 61, 67]. The KKT conditions for problem (1.2) are

$$\begin{aligned} F(X,\boldsymbol{\mu})X := \Big(\nabla f(XX^\top) + \textstyle\sum_{j=1}^m \mu_j W_j\Big) X = X\Sigma, \\ \mathrm{Tr}(X^\top W_j X) = b_j, \quad j = 1,\dots,m, \\ X \in \mathrm{St}_p(\mathbb{R}^n), \quad \Sigma \in \mathbb{S}^p, \quad \mu_j \in \mathbb{R}, \quad j = 1,\dots,m, \end{aligned} \tag{1.4}$$

where $F(X,\boldsymbol{\mu})$ is called the discretized effective Hamiltonian in related fields, $\boldsymbol{\mu} := (\mu_1,\dots,\mu_m)^\top$ and Σ are introduced as the Lagrange multipliers corresponding to the quadratic and manifold constraints, respectively. Given $\boldsymbol{\mu}^{(k)}$, these methods first update $X^{(k)}$ to an intermediate iterate $\tilde{X}^{(k+1)}$ by taking the lowest p eigenvectors of $F(X^{(k)},\boldsymbol{\mu}^{(k)})$[4], which may violate the quadratic constraints. The next iterate $(X^{(k+1)},\boldsymbol{\mu}^{(k+1)})$ is then obtained by approximately solving the subproblem

$$\min_X \ \mathrm{Tr}\Big(X^\top \nabla f\big(\tilde{X}^{(k+1)}(\tilde{X}^{(k+1)})^\top\big)X\Big), \quad \text{s. t. } X \in \mathrm{St}_p(\mathbb{R}^n),\ \mathrm{Tr}(X^\top W_j X) = b_j, \quad j = 1,\dots,m,$$

using a dual Newton method initialized at $\boldsymbol{\mu}^{(k)}$. The Jacobian required in the inner Newton steps can be derived from first-order perturbation theory [61]. Note that the subproblem is constructed by freezing the nonlinear dependence of f on X, which is progressively corrected by the outer-loop intermediate step. Such a double-loop (or nested) methodology may avoid issues related to penalty methods, and has been widely integrated into off-the-shelf codes, e.g., SIESTA [20] and CP2K [41]. Nevertheless, its theoretical properties remain largely unclear. In fact, due to the nonlinearity of f, equation (1.4) does not necessarily imply that X spans

[3] In fact, the exactness is not likely to hold; see our numerical results in Section 4.2.

[4] In practical implementations, direct inversion in the iterative subspace (DIIS) extrapolation is often applied during the outer loop, further modifying the effective operator used to compute $\tilde{X}^{(k+1)}$ [52, 53].

the lowest p-dimensional invariant subspace of $F(X, \boldsymbol{\mu})$ (see [46] for an example), whereas both $\tilde{X}^{(k+1)}$ and $X^{(k+1)}$ are computed via minimization strategies, resulting in a potential mismatch. There would be more subtleties when taking the varying $\boldsymbol{\mu}$ into account. Moreover, the notion of the "lowest" p-dimensional eigenspace is no longer uniquely defined if the eigengap condition $\lambda_{n-p}(F(X, \boldsymbol{\mu})) > \lambda_{n-p+1}(F(X, \boldsymbol{\mu}))$ does not hold, which can lead to oscillations in the iterate sequence. Finally, the overall efficiency and convergence depend critically on the performance of inner Newton steps. In summary, an efficient yet robust numerical algorithm for problem (1.2) is still lacking.

Contributions. To address these gaps, the main contributions of this paper are threefold:

- We propose a subspace-splitting reformulation of problem (1.2) that exploits the inherent rotation invariance of CDFT to decouple the Stiefel manifold constraint from the nonconvex quadratic constraints. Based on this separable structure, we design a single-loop damped subspace splitting algorithm (DASSP) for the reformulated problem.

- We establish the global convergence of DASSP to approximate KKT points under suitable conditions. To the best of our knowledge, our work provides the first algorithm for CDFT calculations with rigorous convergence guarantees, distinguishing it from the two existing classes of methods.

- We demonstrate through extensive experiments on realistic CDFT problems that DASSP achieves superior feasibility accuracy compared to quadratic penalty methods. Furthermore, DASSP exhibits higher computational efficiency than the double-loop method, particularly in systems where eigengap issues typically destabilize standard SCF iterations, without compromising robustness.

We note that the proposed DASSP can be viewed as a damped alternating direction method of multipliers (ADMM). The established theoretical convergence is also worth mentioning compared with recent advances on ADMM-type methods for nonconvex optimization problems, which we briefly review below.

Literature review related to ADMM. Historically, ADMM dates back to the seminal works in the mid-1970s [17, 21] and is deeply rooted in the classical augmented Lagrangian methods (ALM) [29, 51]. While the literature on ADMM and its variants for convex problems is voluminous (see recent surveys [8, 27] and the references therein), the convergence theory for nonconvex and nonlinearly constrained problems is still much less complete. A central theoretical challenge in this context is to ensure the boundedness of the dual iterate sequence [26]. This difficulty is further exacerbated when the constraints are allowed to be nonlinear, as in our case.

Many existing analyses assume the boundedness directly [7, 12, 16, 26, 30]. There are a few exceptions [54, 69]. However, their analyses rely on assumptions that are not aligned with our setting (cf. Eq. (2.1) later): the objective is bounded from below and above [54] (or coercive and partially Lipschitz continuous [69]), the nonlinear constraints are Lipschitz continuous [54, 69] and possibly norm-bounded [54], along with an additional image-inclusion condition on the constraints [69]. Another related line of work concerns Riemannian ADMM [15, 38, 42, 43, 66], which leverages manifold structures explicitly but assumes that any non-manifold constraints are linear and that either the objective is partially Lipschitz continuous or at least one variable block is unconstrained. In our analysis, we address the boundedness issue of the dual iterate sequence by adopting damped dual updates, combined with a careful construction of a surrogate sequence.

Organization. In Section 2, we introduce the subspace-splitting reformulation of problem (1.2) and develop the single-loop DASSP. In Section 3, we establish the convergence properties

of DASSP. Numerical experiments on synthetic and realistic CDFT problems are reported in Section 4. Finally, Section 5 concludes the paper and discusses future directions.

Notation. Let $\mathbb{S}^n$ be the set of $n \times n$ real symmetric matrices. For a matrix A, $A^\top$ denotes its transpose and $\mathrm{Tr}(A)$ denotes its trace. For matrices A and B of the same size, we define the Frobenius inner product by $\langle A, B\rangle := \mathrm{Tr}(A^\top B)$, and denote by $\|A\|_{\mathrm{F}}$ and $\|A\|_2$ the Frobenius norm and spectral norm, respectively. For $A \in \mathbb{S}^n$, its eigenvalues are arranged as $\lambda_1(A) \geq \lambda_2(A) \geq \cdots \geq \lambda_n(A)$. The (real) Stiefel manifold is denoted by $\mathrm{St}_p(\mathbb{R}^n) := \{X \in \mathbb{R}^{n\times p} : X^\top X = I_p\}$. For $X \in \mathrm{St}_p(\mathbb{R}^n)$, we write $\mathrm{P}_X^\perp := I_n - XX^\top$. The notation $\mathrm{Proj}_{\mathcal{C}}(\cdot)$ stands for the Euclidean projection operator onto a closed set $\mathcal{C}$.

2 Algorithmic developments

In this section, we develop the algorithmic framework for problem (1.2). By exploiting the inherent rotation invariance, we first derive a subspace-splitting reformulation that separates the Stiefel manifold constraint from the quadratic constraints. Based on this separable structure, we then propose a damped subspace splitting algorithm.

We have realized that the main difficulty in solving problem (1.2) is due to the presence of two types of constraints for X. A natural idea is to introduce another block of variables and to treat the two groups separately using the alternating direction method of multipliers (ADMM) or its variants.

There are various ways to split the variables, and our goal is to identify a strategy that facilitates the efficient solution of the resulting subproblems. To this end, we notice in problem (1.2) the rotation invariance of both the objective function and the quadratic constraints, namely, they remain unchanged after replacing X with XQ, where $Q \in \mathbb{R}^{p\times p}$ is any orthogonal matrix. In other words, problem (1.2) depends only on the subspace $\mathrm{span}(X)$. This observation motivates us to introduce a matrix variable $Y \in \mathbb{S}^n$ representing the orthogonal projector onto $\mathrm{span}(X)$ directly, at the price of adding a subspace alignment constraint $Y = XX^\top$. We therefore have the following subspace-splitting reformulation of problem (1.2):

$$\min_{X,Y} \; f(Y), \quad \text{s. t. } X \in \mathrm{St}_p(\mathbb{R}^n), \quad Y \in \mathcal{Y}, \quad Y = XX^\top, \tag{2.1}$$

where

$$\mathcal{Y} := \{Y \in \mathbb{S}^n : \mathrm{Tr}(W_j Y) = b_j, \; j = 1, \ldots, m\}. \tag{2.2}$$

This reformulation decouples the two types of constraints in a clean way: the Stiefel manifold constraint remains entirely in the X-block, while the quadratic constraints become linear in the Y-block. We also note that subspace-splitting techniques have been employed in other settings, including distributed principal component analysis [58, 59] and sparse spectral clustering [47].

A straightforward application of ADMM with classical dual updates to problem (2.1) would be problematic due to the introduced nonlinear constraints. As mentioned in Section 1, their presence poses significant challenges when one attempts to show the boundedness of dual iterates [26]. In this work, we propose a variant of ADMM that adopts a damped dual update strategy, called the *damped subspace splitting algorithm* (DASSP).

To begin with, we construct the damped augmented Lagrangian function:

$$\mathcal{L}_{\beta,\delta}(X, Y, \Lambda) := f(Y) + \left\langle (1-\delta)\Lambda, Y - XX^\top \right\rangle + \frac{\beta}{2}\left\| Y - XX^\top \right\|_{\mathrm{F}}^2, \tag{2.3}$$

where $\Lambda \in \mathbb{S}^n$ is the Lagrange multiplier associated with the constraint $Y = XX^\top$, $\beta > 0$ is the penalty parameter, and $\delta \in [0, 1)$ is the damping parameter. Note that the damped augmented

Lagrangian function (2.3) coincides with the standard one when $\delta = 0$. The proposed DASSP updates the variables X, Y, and Λ alternately.

X-update. First, for fixed $Y^{(k)}$ and $\Lambda^{(k)}$, the subproblem for updating X is given by

$$X^{(k+1)} := \underset{X \in \mathrm{St}_p(\mathbb{R}^n)}{\arg\min} \quad \mathcal{L}_{\beta,\delta}(X, Y^{(k)}, \Lambda^{(k)}) = \underset{X \in \mathrm{St}_p(\mathbb{R}^n)}{\arg\min} \quad -\mathrm{Tr}\Big(X^\top A^{(k)} X\Big), \tag{2.4}$$

where

$$A^{(k)} := Y^{(k)} + \frac{1-\delta}{\beta}\Lambda^{(k)} \in \mathbb{S}^n. \tag{2.5}$$

In essence, the X-subproblem (2.4) is an eigenvalue problem of computing an orthonormal basis of the dominant p-dimensional subspace of $A^{(k)}$. This task can be accomplished by direct or iterative eigensolvers [22].

Y-update. Next, for given $X^{(k+1)}$, $Y^{(k)} \in \mathcal{Y}$, and $\Lambda^{(k)}$, we consider the following subproblem over the affine set $\mathcal{Y}$:

$$\begin{aligned} &\min_{Y \in \mathcal{Y}} \quad \mathcal{L}_{\beta,\delta}(X^{(k+1)}, Y, \Lambda^{(k)}) \\ = &\min_{Y \in \mathcal{Y}} \quad f(Y) + \Big\langle (1-\delta)\Lambda^{(k)}, Y - X^{(k+1)}(X^{(k+1)})^\top \Big\rangle + \frac{\beta}{2}\Big\| Y - X^{(k+1)}(X^{(k+1)})^\top \Big\|_{\mathrm{F}}^2. \end{aligned} \tag{2.6}$$

Due to the fact that f could be highly nonlinear, the exact solution to problem (2.6) is out of reach in general. Instead, we perform a single projected gradient step. To this end, let

$$\mathcal{T}_{\mathcal{Y}} := \{Z \in \mathbb{S}^n : \mathrm{Tr}(W_j Z) = 0, \quad j = 1, \ldots, m\}$$

be the tangent space of the affine set $\mathcal{Y}$. Then the update of $Y^{(k+1)}$ takes the form

$$Y^{(k+1)} := Y^{(k)} - \eta_k \mathrm{Proj}_{\mathcal{T}_{\mathcal{Y}}}\Big(\nabla f(Y^{(k)}) + (1-\delta)\Lambda^{(k)} + \beta(Y^{(k)} - X^{(k+1)}(X^{(k+1)})^\top)\Big), \tag{2.7}$$

where $\eta_k > 0$ is the stepsize, $\mathrm{Proj}_{\mathcal{T}_{\mathcal{Y}}} : \mathbb{S}^n \to \mathcal{T}_{\mathcal{Y}}$ is the projection operator onto $\mathcal{T}_{\mathcal{Y}}$, which admits a closed form:

$$\mathrm{Proj}_{\mathcal{T}_{\mathcal{Y}}}(S) := S + \sum_{j=1}^m \hat{\mu}_j W_j, \quad \forall\ S \in \mathbb{S}^n,$$

where the coefficients $\hat{\boldsymbol{\mu}} := (\hat{\mu}_1, \ldots, \hat{\mu}_m)^\top \in \mathbb{R}^m$ are determined by the linear system

$$M\hat{\boldsymbol{\mu}} = -\boldsymbol{c}, \quad \text{with} \quad M_{ij} := \mathrm{Tr}(W_i W_j), \quad c_i := \mathrm{Tr}(W_i S), \quad i, j = 1, \ldots, m. \tag{2.8}$$

The invertibility of the matrix M is implied by Assumption 1.1 (A2). The computational cost of projection is negligible whenever m is small.

Λ-update. Finally, the Lagrange multiplier Λ is updated in a damped dual ascent manner:

$$\Lambda^{(k+1)} := (1-\delta)\Lambda^{(k)} + \tau\beta\Big(Y^{(k+1)} - X^{(k+1)}(X^{(k+1)})^\top\Big), \tag{2.9}$$

where $\tau \in (0, 1]$ is an under-relaxation parameter. The presence of the damping parameter δ is a key feature of the proposed algorithm and plays crucial roles in both algorithmic and theoretical senses. First, the damped dual update (2.9) can be interpreted as a regularized version of the classical dual ascent step. Second, bounding the dual sequence is often the central obstacle in the convergence analysis for nonconvex ADMM-type methods. Intuitively, the damping strategy introduces a contraction effect in equation (2.9), making the dual iterates much easier to control. It also contributes to the construction of a surrogate sequence in the convergence analysis. We note that the damped dual update has recently been used in the ALM literature [25, 36, 49] and the ADMM literature [37, 63, 68] on linearly constrained nonconvex problems. The parameter τ is introduced due to technical reasons and is also observed to be important for numerical stability. Please refer to Sections 3 and 4 for more details.

We outline the proposed DASSP in Algorithm 1.

Algorithm 1: Damped subspace splitting algorithm (DASSP).

Input: Penalty parameter $\beta > 0$, under-relaxation parameter $\tau \in (0, 1]$, damping parameter $\delta \in [0, 1)$, stepsizes $\{\eta_k > 0\}$, initial points $Y^{(0)} \in \mathbb{S}^n$, $\Lambda^{(0)} \in \mathbb{S}^n$.

Set $k := 0$.

if $Y^{(0)} \notin \mathcal{Y}$ **then** project $Y^{(0)}$ onto the affine set $\mathcal{Y}$, i.e., $Y^{(0)} := \mathrm{Proj}_{\mathcal{Y}}(Y^{(0)})$;

while *the stopping criterion is not satisfied* **do**

  Update $X^{(k+1)}$ by solving problem (2.4) with a direct or iterative eigensolver.

  Update $Y^{(k+1)}$ by a single projected gradient step (2.7) with the stepsize η_k.

  Update $\Lambda^{(k+1)}$ by damped dual ascent (2.9).

  Set $k := k + 1$.

Output: $X^{(k)} \in \mathrm{St}_p(\mathbb{R}^n)$.

3 Convergence analysis

In this section, we establish that every accumulation point of the iterate sequence generated by DASSP is an approximate KKT point of problem (1.2), defined as follows.

Definition 3.1. *For a given $\varepsilon > 0$, we say that $X \in \mathbb{R}^{n\times p}$ is an ε-approximate KKT point for problem (1.2) if there exist multipliers $\Sigma \in \mathbb{S}^p$ and $\boldsymbol{\mu} \in \mathbb{R}^m$ such that*

$$\max\left\{\|F(X,\boldsymbol{\mu})X - X\Sigma\|_{\mathrm{F}}, \left\|X^\top X - I_p\right\|_{\mathrm{F}}, \max_{1\le j\le m}\left|\mathrm{Tr}(X^\top W_j X) - b_j\right|\right\} \le \varepsilon,$$

where $F(X,\boldsymbol{\mu})$ is defined in equation (1.4).

We now list the assumptions for the convergence analysis.

Assumption 3.1. *Given the damping parameter $\delta \in (0, 1)$, let c be a constant satisfying $c > 2(1-\delta)(2-\delta)/\delta$.*

(A1) *The objective function $f : \mathbb{S}^n \to \mathbb{R}$ is continuously differentiable and L-smooth, i.e., there exists an $L > 0$ such that*

$$\|\nabla f(U) - \nabla f(V)\|_{\mathrm{F}} \le L\|U - V\|_{\mathrm{F}}, \quad \forall\, U, V \in \mathbb{S}^n.$$

(A2) *The sequence $\{A^{(k)}\}_{k\ge 0}$ defined in equation (2.5) has a uniform eigengap, i.e., there exists a $\gamma > 0$ such that*

$$\gamma_k := \lambda_p(A^{(k)}) - \lambda_{p+1}(A^{(k)}) \ge \gamma, \quad \forall\, k \in \mathbb{N}.$$

(A3) *The penalty parameter β satisfies $\beta > 2(L + 1)$, where L is defined in (A1).*

(A4) *The stepsize $\eta_k \equiv \eta$ satisfies $\eta \in (0, 2/(\beta + L))$.*

(A5) *The under-relaxation parameter τ satisfies*

$$\tau \in \left(0, \frac{\delta}{2c}\min\left\{\frac{1}{\beta}\left(\frac{1}{\eta} - \frac{\beta + L}{2}\right), \frac{\gamma}{n}\right\}\right),$$

where γ is defined in (A2).

Remark 3.1. Assumption 3.1 (A2) is a standard condition commonly used in the literature to guarantee the well-posedness of the linear eigenvalue problem (2.4) throughout the iterations [4, 45, 46]. Although we cannot remove it in the current analysis, we remark that it holds when $Y^{(k)}$ and $\Lambda^{(k)}$ are sufficiently close to fixed matrices $\bar{X}\bar{X}^\top \in \mathbb{S}^n$ and $\bar{\Lambda} \in \mathbb{S}^n$ with $\bar{X} \in \mathrm{St}_p(\mathbb{R}^n)$, and β is sufficiently large; this can be shown by using the perturbation theory of matrix eigenvalues [22]. We also provide supporting numerical evidence in Section 4.4. In Assumption 3.1 (A4), the stepsize is assumed to be constant for simplicity. An extension of our analysis to cases with variable stepsizes $\eta_k \in [\varepsilon_0, 2/(\beta+L)-\varepsilon_0]$ for any fixed $\varepsilon_0 > 0$ would be straightforward but tedious.

Let $\{(X^{(k)}, Y^{(k)}, \Lambda^{(k)})\}$ be the sequence generated by Algorithm 1. Throughout this section, we denote the subspace alignment violation by

$$R^{(k)} := Y^{(k)} - X^{(k)}(X^{(k)})^\top \in \mathbb{S}^n. \tag{3.1}$$

We first quantify the decrease in the damped augmented Lagrangian induced by primal updates.

Lemma 3.1. *Suppose that* Assumption 3.1 (A2) *holds. Then, for every* $k \geq 0$,

$$\mathcal{L}_{\beta,\delta}(X^{(k+1)}, Y^{(k)}, \Lambda^{(k)}) - \mathcal{L}_{\beta,\delta}(X^{(k)}, Y^{(k)}, \Lambda^{(k)}) \leq -\frac{\beta\gamma}{n} \left\| X^{(k+1)}(X^{(k+1)})^\top - X^{(k)}(X^{(k)})^\top \right\|_{\mathrm{F}}^2.$$

Proof. A direct calculation yields

$$\begin{aligned} &\mathcal{L}_{\beta,\delta}(X^{(k+1)}, Y^{(k)}, \Lambda^{(k)}) - \mathcal{L}_{\beta,\delta}(X^{(k)}, Y^{(k)}, \Lambda^{(k)}) \\ =\ & -\beta \left(\mathrm{Tr}((X^{(k+1)})^\top A^{(k)} X^{(k+1)}) - \mathrm{Tr}((X^{(k)})^\top A^{(k)} X^{(k)}) \right). \end{aligned}$$

Since $X^{(k)}, X^{(k+1)} \in \mathrm{St}_p(\mathbb{R}^n)$, applying [45, Lemma 3.1] to $-A^{(k)}$, and using Assumption 3.1 (A2), we obtain

$$\begin{aligned} \mathcal{L}_{\beta,\delta}(X^{(k+1)}, Y^{(k)}, \Lambda^{(k)}) - \mathcal{L}_{\beta,\delta}(X^{(k)}, Y^{(k)}, \Lambda^{(k)}) &\leq -\beta\gamma \left\| X^{(k+1)}(X^{(k+1)})^\top - X^{(k)}(X^{(k)})^\top \right\|_2^2 \\ &\leq -\frac{\beta\gamma}{n} \left\| X^{(k+1)}(X^{(k+1)})^\top - X^{(k)}(X^{(k)})^\top \right\|_{\mathrm{F}}^2, \end{aligned}$$

which completes the proof. □

Lemma 3.2. *Suppose that* Assumption 3.1 (A1) *and* (A4) *hold. Then, for every* $k \geq 0$,

$$\mathcal{L}_{\beta,\delta}(X^{(k+1)}, Y^{(k+1)}, \Lambda^{(k)}) - \mathcal{L}_{\beta,\delta}(X^{(k+1)}, Y^{(k)}, \Lambda^{(k)}) \leq -\left(\frac{1}{\eta} - \frac{\beta+L}{2}\right) \left\| Y^{(k+1)} - Y^{(k)} \right\|_{\mathrm{F}}^2.$$

Proof. For fixed $X^{(k+1)}$ and $\Lambda^{(k)}$, the gradient of the damped augmented Lagrangian with respect to Y is given by

$$\nabla_Y \mathcal{L}_{\beta,\delta}(X^{(k+1)}, Y, \Lambda^{(k)}) = \nabla f(Y) + (1-\delta)\Lambda^{(k)} + \beta(Y - X^{(k+1)}(X^{(k+1)})^\top),$$

which is $(\beta + L)$-Lipschitz continuous by Assumption 3.1 (A1). Let

$$G^{(k)} := \mathrm{Proj}_{\mathcal{T}_{\mathcal{Y}}} \left(\nabla f(Y^{(k)}) + (1-\delta)\Lambda^{(k)} + \beta(Y^{(k)} - X^{(k+1)}(X^{(k+1)})^\top) \right). \tag{3.2}$$

Then the Y-update gives $Y^{(k+1)} - Y^{(k)} = -\eta G^{(k)} \in \mathcal{T}_{\mathcal{Y}}$. By the standard descent lemma,

$$\begin{aligned} &\mathcal{L}_{\beta,\delta}(X^{(k+1)}, Y^{(k+1)}, \Lambda^{(k)}) - \mathcal{L}_{\beta,\delta}(X^{(k+1)}, Y^{(k)}, \Lambda^{(k)}) \\ \leq\ & \left\langle \nabla_Y \mathcal{L}_{\beta,\delta}(X^{(k+1)}, Y^{(k)}, \Lambda^{(k)}), Y^{(k+1)} - Y^{(k)} \right\rangle + \frac{\beta+L}{2} \left\| Y^{(k+1)} - Y^{(k)} \right\|_{\mathrm{F}}^2 \\ =\ & -\frac{1}{\eta} \left\| Y^{(k+1)} - Y^{(k)} \right\|_{\mathrm{F}}^2 + \frac{\beta+L}{2} \left\| Y^{(k+1)} - Y^{(k)} \right\|_{\mathrm{F}}^2 = -\left(\frac{1}{\eta} - \frac{\beta+L}{2}\right) \left\| Y^{(k+1)} - Y^{(k)} \right\|_{\mathrm{F}}^2. \end{aligned}$$

This completes the proof. □

Next, we turn to the behavior of the dual updates. To facilitate the analysis, we introduce an auxiliary sequence

$$T_k := \mathcal{L}_{\beta,\delta}(X^{(k)}, Y^{(k)}, \Lambda^{(k)}) - \frac{\delta(1-\delta)}{2\tau\beta}\|\Lambda^{(k)}\|_{\mathrm{F}}^2. \tag{3.3}$$

The following lemma provides an upper bound for $T_{k+1} - T_k$.

Lemma 3.3. *Suppose that* Assumption 3.1 (A1), (A2), and (A4) *hold. Then, for every* $k \geq 0$,

$$\begin{aligned} T_{k+1} - T_k \leq & -\left(\frac{1}{\eta} - \frac{\beta + L}{2}\right)\left\|Y^{(k+1)} - Y^{(k)}\right\|_{\mathrm{F}}^2 - \frac{\beta\gamma}{n}\left\|X^{(k+1)}(X^{(k+1)})^\top - X^{(k)}(X^{(k)})^\top\right\|_{\mathrm{F}}^2 \\ & + \frac{(1-\delta)(1-\frac{\delta}{2})}{\tau\beta}\left\|\Lambda^{(k+1)} - \Lambda^{(k)}\right\|_{\mathrm{F}}^2. \end{aligned}$$

Proof. By direct calculation, we have

$$\mathcal{L}_{\beta,\delta}(X^{(k+1)}, Y^{(k+1)}, \Lambda^{(k+1)}) - \mathcal{L}_{\beta,\delta}(X^{(k+1)}, Y^{(k+1)}, \Lambda^{(k)}) = (1-\delta)\left\langle \Lambda^{(k+1)} - \Lambda^{(k)}, R^{(k+1)} \right\rangle.$$

Using the dual update (2.9), we obtain

$$R^{(k+1)} = \frac{1}{\tau\beta}\left(\Lambda^{(k+1)} - (1-\delta)\Lambda^{(k)}\right). \tag{3.4}$$

Hence,

$$(1-\delta)\left\langle \Lambda^{(k+1)} - \Lambda^{(k)}, R^{(k+1)} \right\rangle = \frac{1-\delta}{\tau\beta}\left\langle \Lambda^{(k+1)} - \Lambda^{(k)}, \Lambda^{(k+1)} - (1-\delta)\Lambda^{(k)} \right\rangle.$$

A direct expansion gives

$$\begin{aligned} & (1-\delta)\left\langle \Lambda^{(k+1)} - \Lambda^{(k)}, R^{(k+1)} \right\rangle - \frac{\delta(1-\delta)}{2\tau\beta}\left(\|\Lambda^{(k+1)}\|_{\mathrm{F}}^2 - \|\Lambda^{(k)}\|_{\mathrm{F}}^2\right) \\ = & \frac{(1-\delta)(1-\frac{\delta}{2})}{\tau\beta}\left\|\Lambda^{(k+1)} - \Lambda^{(k)}\right\|_{\mathrm{F}}^2. \end{aligned}$$

Combining this identity with Lemmas 3.1 and 3.2 yields the desired inequality. □

The upper bound in Lemma 3.3 contains a positive term arising from the dual update, which cannot be easily controlled by telescoping arguments. To handle this, we exploit the dual update (2.9) to relate the dual differences to the primal differences.

Lemma 3.4. *For any* $\varepsilon_X, \varepsilon_Y > 0$, *and any* $k \geq 1$, *the following inequality holds*

$$\begin{aligned} \frac{1-\delta}{2\tau\beta}\left\|\Lambda^{(k+1)} - \Lambda^{(k)}\right\|_{\mathrm{F}}^2 \leq & \frac{1-\delta}{2\tau\beta}\left\|\Lambda^{(k)} - \Lambda^{(k-1)}\right\|_{\mathrm{F}}^2 - \left(\frac{\delta}{2\tau\beta} - \frac{1}{2\varepsilon_Y} - \frac{1}{2\varepsilon_X}\right)\left\|\Lambda^{(k+1)} - \Lambda^{(k)}\right\|_{\mathrm{F}}^2 \\ & + \frac{\varepsilon_Y}{2}\left\|Y^{(k+1)} - Y^{(k)}\right\|_{\mathrm{F}}^2 + \frac{\varepsilon_X}{2}\left\|X^{(k+1)}(X^{(k+1)})^\top - X^{(k)}(X^{(k)})^\top\right\|_{\mathrm{F}}^2. \end{aligned}$$

Proof. From equation (3.4), we obtain

$$R^{(k+1)} - R^{(k)} = \frac{1}{\tau\beta}\left((\Lambda^{(k+1)} - \Lambda^{(k)}) - (1-\delta)(\Lambda^{(k)} - \Lambda^{(k-1)})\right).$$

Taking inner products with $2\tau\beta(\Lambda^{(k+1)} - \Lambda^{(k)})$ on both sides gives

$$2\tau\beta\left\langle \Lambda^{(k+1)} - \Lambda^{(k)}, R^{(k+1)} - R^{(k)} \right\rangle$$

$$
\begin{aligned}
&= 2\left\langle \Lambda^{(k+1)} - \Lambda^{(k)}, (\Lambda^{(k+1)} - \Lambda^{(k)}) - (1-\delta)(\Lambda^{(k)} - \Lambda^{(k-1)}) \right\rangle \\
&= \left\| (\Lambda^{(k+1)} - \Lambda^{(k)}) - (1-\delta)(\Lambda^{(k)} - \Lambda^{(k-1)}) \right\|_{\mathrm{F}}^2 + \left\| \Lambda^{(k+1)} - \Lambda^{(k)} \right\|_{\mathrm{F}}^2 - (1-\delta)^2 \left\| \Lambda^{(k)} - \Lambda^{(k-1)} \right\|_{\mathrm{F}}^2 \\
&\geq \left\| \Lambda^{(k+1)} - \Lambda^{(k)} \right\|_{\mathrm{F}}^2 - (1-\delta)^2 \left\| \Lambda^{(k)} - \Lambda^{(k-1)} \right\|_{\mathrm{F}}^2 .
\end{aligned}
$$

After rearranging, we arrive at

$$
\begin{aligned}
&\frac{1-\delta}{2\tau\beta} \left\| \Lambda^{(k+1)} - \Lambda^{(k)} \right\|_{\mathrm{F}}^2 \\
&\leq \frac{(1-\delta)^2}{2\tau\beta} \left\| \Lambda^{(k)} - \Lambda^{(k-1)} \right\|_{\mathrm{F}}^2 + \left\langle \Lambda^{(k+1)} - \Lambda^{(k)}, R^{(k+1)} - R^{(k)} \right\rangle - \frac{\delta}{2\tau\beta} \left\| \Lambda^{(k+1)} - \Lambda^{(k)} \right\|_{\mathrm{F}}^2 \qquad (3.5) \\
&\leq \frac{1-\delta}{2\tau\beta} \left\| \Lambda^{(k)} - \Lambda^{(k-1)} \right\|_{\mathrm{F}}^2 + \left\langle \Lambda^{(k+1)} - \Lambda^{(k)}, R^{(k+1)} - R^{(k)} \right\rangle - \frac{\delta}{2\tau\beta} \left\| \Lambda^{(k+1)} - \Lambda^{(k)} \right\|_{\mathrm{F}}^2 .
\end{aligned}
$$

For arbitrary $\varepsilon_X, \varepsilon_Y > 0$, it follows from Young's inequality that

$$
\left\langle \Lambda^{(k+1)} - \Lambda^{(k)}, Y^{(k+1)} - Y^{(k)} \right\rangle \leq \frac{\varepsilon_Y}{2} \left\| Y^{(k+1)} - Y^{(k)} \right\|_{\mathrm{F}}^2 + \frac{1}{2\varepsilon_Y} \left\| \Lambda^{(k+1)} - \Lambda^{(k)} \right\|_{\mathrm{F}}^2
$$

and

$$
\begin{aligned}
&- \left\langle \Lambda^{(k+1)} - \Lambda^{(k)}, X^{(k+1)}(X^{(k+1)})^\top - X^{(k)}(X^{(k)})^\top \right\rangle \\
&\leq \frac{\varepsilon_X}{2} \left\| X^{(k+1)}(X^{(k+1)})^\top - X^{(k)}(X^{(k)})^\top \right\|_{\mathrm{F}}^2 + \frac{1}{2\varepsilon_X} \left\| \Lambda^{(k+1)} - \Lambda^{(k)} \right\|_{\mathrm{F}}^2 .
\end{aligned}
$$

Substituting the above inequalities into equation (3.5), we complete the proof. □

By invoking Lemma 3.4, the positive term in Lemma 3.3 can be controlled after properly choosing parameters. Based on this, we construct the following surrogate sequence to monitor the behavior of the algorithm:

$$
\Psi_k := T_k + c \cdot \frac{1-\delta}{2\tau\beta} \left\| \Lambda^{(k)} - \Lambda^{(k-1)} \right\|_{\mathrm{F}}^2 + C_0, \qquad (3.6)
$$

where T_k is defined in equation (3.3), the constant c is given in Assumption 3.1, and C_0 is defined as

$$
C_0 := \frac{1}{2} \|\nabla f(0)\|_{\mathrm{F}}^2 + (L+1)p - f(0),
$$

which ensures the lower boundedness of $\{\Psi_k\}$ (see Lemma 3.6). The next lemma establishes a descent inequality for $\{\Psi_k\}$.

Lemma 3.5. *Suppose that* Assumption 3.1 *holds. Then there exist constants $c_1, c_2, c_3 > 0$ such that*

$$
\Psi_{k+1} - \Psi_k \leq -c_1 \left\| Y^{(k+1)} - Y^{(k)} \right\|_{\mathrm{F}}^2 - c_2 \left\| X^{(k+1)}(X^{(k+1)})^\top - X^{(k)}(X^{(k)})^\top \right\|_{\mathrm{F}}^2 - c_3 \left\| \Lambda^{(k+1)} - \Lambda^{(k)} \right\|_{\mathrm{F}}^2 \qquad (3.7)
$$

holds for all $k \geq 1$.

Proof. Combining Lemma 3.3 with Lemma 3.4, we obtain

$$
\begin{aligned}
\Psi_{k+1} - \Psi_k \leq & - \left(\frac{1}{\eta} - \frac{\beta + L}{2} - \frac{c \cdot \varepsilon_Y}{2} \right) \left\| Y^{(k+1)} - Y^{(k)} \right\|_{\mathrm{F}}^2 \\
& - \left(\frac{\beta\gamma}{n} - \frac{c \cdot \varepsilon_X}{2} \right) \left\| X^{(k+1)}(X^{(k+1)})^\top - X^{(k)}(X^{(k)})^\top \right\|_{\mathrm{F}}^2
\end{aligned}
$$

$$- \left(c\left(\frac{\delta}{2\tau\beta} - \frac{1}{2\varepsilon_Y} - \frac{1}{2\varepsilon_X} \right) - \frac{(1-\delta)(1-\frac{\delta}{2})}{\tau\beta} \right) \left\| \Lambda^{(k+1)} - \Lambda^{(k)} \right\|_{\mathrm{F}}^2.$$

Next, we choose $\varepsilon_X = \varepsilon_Y = 4\tau\beta/\delta > 0$. Substituting this choice into the above estimate yields equation (3.7) with

$$c_1 := \frac{1}{\eta} - \frac{\beta + L}{2} - \frac{2c\tau\beta}{\delta}, \quad c_2 := \left(\frac{\gamma}{n} - \frac{2c\tau}{\delta} \right) \beta, \quad c_3 := \frac{1}{\tau\beta} \left(\frac{c\delta}{4} - (1-\delta)\left(1 - \frac{\delta}{2}\right) \right).$$

The positivity of these constants follows from the condition $c > 2(1-\delta)(2-\delta)/\delta$, together with the bound on τ in Assumption 3.1 (A5). □

The next step is to show that $\{\Psi_k\}$ is bounded from below.

Lemma 3.6. *Suppose that* Assumption 3.1 *holds. Then the sequence* $\{\Psi_k\}$ *is bounded from below.*

Proof. We decompose Ψ_k into two parts:

$$\Psi_k = \underbrace{f(Y^{(k)}) + \frac{\beta}{2} \left\| R^{(k)} \right\|_{\mathrm{F}}^2 + \frac{\delta(1-\delta)}{2\tau\beta} \left\| \Lambda^{(k)} \right\|_{\mathrm{F}}^2 + c \cdot \frac{1-\delta}{2\tau\beta} \left\| \Lambda^{(k)} - \Lambda^{(k-1)} \right\|_{\mathrm{F}}^2 + C_0}_{\text{Part 1}}$$
$$+ \underbrace{\left\langle (1-\delta)\Lambda^{(k)}, R^k \right\rangle - \frac{\delta(1-\delta)}{\tau\beta} \left\| \Lambda^{(k)} \right\|_{\mathrm{F}}^2}_{\text{Part 2}}.$$

For Part 1, we first estimate the objective term. By Assumption 3.1 (A1),

$$f(Y^{(k)}) \geq f(0) + \left\langle \nabla f(0), Y^{(k)} \right\rangle - \frac{L}{2} \left\| Y^{(k)} \right\|_{\mathrm{F}}^2 \geq -\frac{L+1}{2} \left\| Y^{(k)} \right\|_{\mathrm{F}}^2 - \frac{1}{2} \left\| \nabla f(0) \right\|_{\mathrm{F}}^2 + f(0).$$

Since $R^{(k)} = Y^{(k)} - X^{(k)}(X^{(k)})^\top$ and $\left\| X^{(k)}(X^{(k)})^\top \right\|_{\mathrm{F}}^2 = p$, we have $\left\| Y^{(k)} \right\|_{\mathrm{F}}^2 \leq 2(\left\| R^{(k)} \right\|_{\mathrm{F}}^2 + p)$. Therefore, by Assumption 3.1 (A3),

$$\text{Part 1} \geq f(Y^{(k)}) + \frac{\beta}{2} \left\| R^{(k)} \right\|_{\mathrm{F}}^2 + C_0 \geq \left(\frac{\beta}{2} - L - 1 \right) \left\| R^{(k)} \right\|_{\mathrm{F}}^2 \geq 0.$$

For Part 2, it follows from direct calculations that

$$\begin{aligned} \text{Part 2} &= \left\langle (1-\delta)\Lambda^{(k)}, \frac{\Lambda^{(k)} - (1-\delta)\Lambda^{(k-1)}}{\tau\beta} - \frac{\delta}{\tau\beta}\Lambda^{(k)} \right\rangle \\ &= \frac{(1-\delta)^2}{2\tau\beta} \left(\left\| \Lambda^{(k)} \right\|_{\mathrm{F}}^2 - \left\| \Lambda^{(k-1)} \right\|_{\mathrm{F}}^2 + \left\| \Lambda^{(k)} - \Lambda^{(k-1)} \right\|_{\mathrm{F}}^2 \right) \\ &\geq \frac{(1-\delta)^2}{2\tau\beta} \left(\left\| \Lambda^{(k)} \right\|_{\mathrm{F}}^2 - \left\| \Lambda^{(k-1)} \right\|_{\mathrm{F}}^2 \right). \end{aligned}$$

Combining the estimates of Part 1 and Part 2, we obtain

$$\Psi_k \geq \frac{(1-\delta)^2}{2\tau\beta} \left(\left\| \Lambda^{(k)} \right\|_{\mathrm{F}}^2 - \left\| \Lambda^{(k-1)} \right\|_{\mathrm{F}}^2 \right).$$

For any $K \geq 1$, summing the above inequality from $k = 1$ to K yields

$$\sum_{k=1}^{K} \Psi_k \geq \frac{(1-\delta)^2}{2\tau\beta} \left(\left\| \Lambda^{(K)} \right\|_{\mathrm{F}}^2 - \left\| \Lambda^{(0)} \right\|_{\mathrm{F}}^2 \right) \geq -\frac{(1-\delta)^2}{2\tau\beta} \left\| \Lambda^{(0)} \right\|_{\mathrm{F}}^2.$$

Hence, $\{\sum_{k=1}^{K} \Psi_k\}$ is bounded below. Together with the fact that $\{\Psi_k\}$ is nonincreasing from Lemma 3.5, we conclude that $\Psi_k \geq 0$ for all $k \geq 1$. □

An immediate consequence of Lemmas 3.5 and 3.6 is as follows.

Corollary 3.1. *Suppose that* Assumption 3.1 *holds. Then*

$$\sum_{k=1}^{\infty}\left\|Y^{(k+1)}-Y^{(k)}\right\|_{\mathrm{F}}^2,\quad \sum_{k=1}^{\infty}\left\|X^{(k+1)}(X^{(k+1)})^\top-X^{(k)}(X^{(k)})^\top\right\|_{\mathrm{F}}^2,\quad \sum_{k=1}^{\infty}\left\|\Lambda^{(k+1)}-\Lambda^{(k)}\right\|_{\mathrm{F}}^2$$

are all finite. In particular, $Y^{(k+1)}-Y^{(k)}\to 0$, $X^{(k+1)}(X^{(k+1)})^\top-X^{(k)}(X^{(k)})^\top\to 0$, $\Lambda^{(k+1)}-\Lambda^{(k)}\to 0$. *Moreover, we have* $G^{(k)}\to 0$.

The remaining issue is to establish the boundedness of iterates.

Lemma 3.7. *Under* Assumption 3.1, *the sequences* $\{Y^{(k)}\}$ *and* $\{\Lambda^{(k)}\}$ *generated by Algorithm 1 are bounded.*

Proof. In the proof of Lemma 3.6, we have established that

$$\Psi_k\geq\frac{\delta(1-\delta)}{2\tau\beta}\left\|\Lambda^{(k)}\right\|_{\mathrm{F}}^2+\frac{(1-\delta)^2}{2\tau\beta}\left(\left\|\Lambda^{(k)}\right\|_{\mathrm{F}}^2-\left\|\Lambda^{(k-1)}\right\|_{\mathrm{F}}^2\right).$$

Since $\{\Psi_k\}$ is nonincreasing, we have $\Psi_k\leq\Psi_1$, which further implies

$$\left\|\Lambda^{(k)}\right\|_{\mathrm{F}}^2\leq(1-\delta)\left\|\Lambda^{(k-1)}\right\|_{\mathrm{F}}^2+\frac{2\tau\beta}{1-\delta}\Psi_1.$$

Applying this inequality recursively gives

$$\left\|\Lambda^{(k)}\right\|_{\mathrm{F}}^2\leq(1-\delta)^k\left\|\Lambda^{(0)}\right\|_{\mathrm{F}}^2+\frac{2\tau\beta}{1-\delta}\Psi_1\sum_{\ell=0}^{k-1}(1-\delta)^\ell\leq\left\|\Lambda^{(0)}\right\|_{\mathrm{F}}^2+\frac{2\tau\beta}{\delta(1-\delta)}\Psi_1.$$

Thus, $\{\Lambda^{(k)}\}$ is bounded. Finally, we rewrite the dual update (2.9) as

$$Y^{(k)}=X^{(k)}(X^{(k)})^\top+\frac{1}{\tau\beta}\left(\Lambda^{(k)}-(1-\delta)\Lambda^{(k-1)}\right).$$

Since $\left\|X^{(k)}(X^{(k)})^\top\right\|_{\mathrm{F}}=\sqrt{p}$ and $\{\Lambda^{(k)}\}$ is bounded, the sequence $\{Y^{(k)}\}$ is bounded as well. □

We now state the main convergence result for Algorithm 1.

Theorem 3.1. *Suppose that* Assumption 3.1 *holds. Let* $\{(X^{(k)},Y^{(k)},\Lambda^{(k)})\}$ *be the sequence generated by Algorithm 1. Then* $\{(X^{(k)},Y^{(k)},\Lambda^{(k)})\}$ *has at least one accumulation point, and for each accumulation point* $(X^\star,Y^\star,\Lambda^\star)$, *there exist multipliers* $\Sigma^\star\in\mathbb{S}^p$ *and* $\boldsymbol{\mu}^\star=(\mu_1^\star,\ldots,\mu_m^\star)^\top\in\mathbb{R}^m$ *such that*

$$\left\|F(X^\star,\boldsymbol{\mu}^\star)X^\star-X^\star\Sigma^\star\right\|_{\mathrm{F}}\leq\hat{C}_1\delta,\qquad\max_{1\leq j\leq m}\left|\mathrm{Tr}(X^{\star\top}W_jX^\star)-b_j\right|\leq\hat{C}_2\delta,$$

where

$$\hat{C}_1:=\frac{L\sqrt{p(n-p)}}{\tau\beta}\left\|\Lambda^\star\right\|_{\mathrm{F}},\quad\hat{C}_2:=\frac{1}{\tau\beta}\left\|\Lambda^\star\right\|_{\mathrm{F}}\cdot\max_{1\leq j\leq m}\left\|W_j\right\|_{\mathrm{F}}.$$

Proof. The existence of an accumulation point follows directly from Lemma 3.7 and the compactness of the Stiefel manifold. By equation (3.2) and the characterization of the orthogonal projection onto $\mathcal{T}_\mathcal{Y}$, there exists a unique matrix $N^{(k)}\in\mathrm{span}\{W_1,\ldots,W_m\}$ such that

$$G^{(k)}=\nabla f(Y^{(k)})+(1-\delta)\Lambda^{(k)}+\beta(Y^{(k)}-X^{(k+1)}(X^{(k+1)})^\top)+N^{(k)}.\tag{3.8}$$

Since $\|G^{(k)}\|_{\mathrm{F}} \to 0$, $\{X^{(k)}\}, \{Y^{(k)}\}$ and $\{\Lambda^{(k)}\}$ are bounded, we have that $\{N^{(k)}\}$ is bounded as well. We further define

$$\Sigma^{(k)} := (X^{(k)})^\top \Big(\nabla f(X^{(k)}(X^{(k)})^\top) + N^{(k)}\Big) X^{(k)} \in \mathbb{S}^p. \tag{3.9}$$

Passing to a convergent subsequence without relabeling, we may assume $X^{(k)} \to X^\star \in \mathrm{St}_p(\mathbb{R}^n)$, $Y^{(k)} \to Y^\star \in \mathcal{Y}$, $\Lambda^{(k)} \to \Lambda^\star$, $\Sigma^{(k)} \to \Sigma^\star$, and $N^{(k)} \to N^\star = \sum_{j=1}^m \mu_j^\star W_j \in \mathbb{S}^n$ for some $\boldsymbol{\mu}^\star \in \mathbb{R}^m$.

It follows from equations (3.8) and (3.9) that

$$\begin{aligned}
&\Big(\nabla f(X^{(k)}(X^{(k)})^\top) + N^{(k)}\Big) X^{(k)} - X^{(k)}\Sigma^{(k)} \\
&= \mathrm{P}^\perp_{X^{(k)}} \Big(\nabla f(X^{(k)}(X^{(k)})^\top) + N^{(k)}\Big) X^{(k)} \\
&= \mathrm{P}^\perp_{X^{(k)}} \Big(-\beta(Y^{(k)} - X^{(k+1)}(X^{(k+1)})^\top) - (1-\delta)\Lambda^{(k)}\Big) X^{(k)} \\
&\quad + \mathrm{P}^\perp_{X^{(k)}} \Big(G^{(k)} + \nabla f(X^{(k)}(X^{(k)})^\top) - \nabla f(Y^{(k)})\Big) X^{(k)}.
\end{aligned} \tag{3.10}$$

Note that the first term on the right-hand side vanishes as $k \to \infty$ by Corollary 3.1 and

$$\mathrm{P}^\perp_{X^{(k+1)}} \Big(\beta(Y^{(k)} - X^{(k+1)}(X^{(k+1)})^\top) + (1-\delta)\Lambda^{(k)}\Big) X^{(k+1)} = 0,$$

which follows from the first-order optimality condition of the X-subproblem (2.4). For the second term, by Assumption 3.1 (A1), we have

$$\Big\|\mathrm{P}^\perp_{X^{(k)}} \Big(G^{(k)} + \nabla f(X^{(k)}(X^{(k)})^\top) - \nabla f(Y^{(k)})\Big) X^{(k)}\Big\|_{\mathrm{F}} \le \sqrt{p(n-p)}\Big(\big\|G^{(k)}\big\|_{\mathrm{F}} + L \big\|R^{(k)}\big\|_{\mathrm{F}}\Big).$$

Taking the limit $k \to \infty$ in equation (3.10) and using both Corollary 3.1 and equation (3.4), we arrive at

$$\|F(X^\star, \boldsymbol{\mu}^\star)X^\star - X^\star\Sigma^\star\| = \Big\|\Big(\nabla f(X^\star X^{\star\top}) + N^\star\Big)X^\star - X^\star\Sigma^\star\Big\|_{\mathrm{F}} \le \frac{L\sqrt{p(n-p)}}{\tau\beta} \|\Lambda^\star\|_{\mathrm{F}}\, \delta.$$

For feasibility, since $Y^\star \in \mathcal{Y}$, we have $\mathrm{Tr}(W_j Y^\star) = b_j$ for $j = 1, \ldots, m$. Hence

$$\Big|\mathrm{Tr}(X^{\star\top} W_j X^\star) - b_j\Big| = \Big|\mathrm{Tr}(W_j(X^\star X^{\star\top} - Y^\star))\Big| \le \|W_j\|_{\mathrm{F}} \|R^\star\|_{\mathrm{F}} = \frac{\delta}{\tau\beta} \|\Lambda^\star\|_{\mathrm{F}} \|W_j\|_{\mathrm{F}}.$$

Taking the maximum over j gives the feasibility bound and completes the proof. □

4 Numerical experiments

In this section, we test the proposed DASSP on synthetic and realistic CDFT problems. In Section 4.1, we determine a default setting of parameters in DASSP by experiments on synthetic test instances. In Sections 4.2-4.4, we demonstrate the effectiveness, efficiency, and robustness of DASSP on charge-transfer and charge-localization problems, through numerical comparison with two classes of algorithms mentioned in Section 1.

Algorithms in comparison. The first class is the quadratic penalty method [39, 40, 48]. As discussed in Section 1, the penalty problem (1.3) can be solved by either the SCF iteration or optimization algorithms on the Stiefel manifold. The former option is abbreviated as QP-SCF and is implemented using the PySCF package [55]. For the latter, we invoke the PCAL algorithm on the Stiefel manifold with its default setting [18, 19] and call the resulting method QP-PCAL. The second class is the double-loop method proposed by Wu and Van Voorhis [61], referred to as

the WV method. Its implementation follows from the CDFT example in the PySCF package[5]. We further employ the post-DIIS method [52, 53] with a subspace dimension of eight in both the QP-SCF and WV methods for acceleration.

Stopping criteria. We define the following two residuals: for any $X \in \mathbb{R}^{n\times p}$ and $\boldsymbol{\mu} \in \mathbb{R}^m$,

$$r_1(X, \boldsymbol{\mu}) := \left\|(I - XX^\top)F(X, \boldsymbol{\mu})X\right\|_{\mathrm{F}}, \quad r_2(X) := \max_{1\le j\le m} \left|\mathrm{Tr}\big(X^\top W_j X\big) - b_j\right|.$$

The former denotes the stationarity (resp., substationarity) violation for the QP-SCF and QP-PCAL (resp., WV and DASSP) methods (cf. equation (1.4) with $\Sigma := X^\top F(X, \boldsymbol{\mu})X$), while the latter represents the feasibility violation for the WV and DASSP methods. Unless otherwise specified, the QP-SCF and QP-PCAL are declared converged when $r_1\big(X^{(k)}, \tilde{\boldsymbol{\mu}}^{(k)}\big)$ falls below 10^{-8}, where $\tilde{\boldsymbol{\mu}}^{(k)} := (\tilde{\mu}_1^{(k)}, \ldots, \tilde{\mu}_m^{(k)})^\top \in \mathbb{R}^m$ and $\tilde{\mu}_j^{(k)} := 2\sigma(\mathrm{Tr}((X^{(k)})^\top W_j X^{(k)}) - b_j)$ $(j = 1, \ldots, m)$. Moreover, an orthogonalization post-processing step is enabled for QP-PCAL when the final manifold constraint violation exceeds 10^{-13} [18]. In the WV method, the inner Newton step is terminated when $r_2(X^{(k)})$ falls below 10^{-8} or the inner iteration number exceeds a prespecified value; at most 20 inner Newton steps are allowed during the first ten outer iterations, and at most 50 inner steps are allowed thereafter. The outer iteration is terminated when $r_1\big(X^{(k)}, \boldsymbol{\mu}^{(k)}\big)$ is smaller than 10^{-8}; see Section 1 for the definition of $\boldsymbol{\mu}^{(k)}$. DASSP is terminated when $r_1\big(X^{(k)}, \hat{\boldsymbol{\mu}}^{(k)}\big)$ and $r_2(X^{(k)})$ are both below 10^{-8}, where $\hat{\boldsymbol{\mu}}^{(k)} \in \mathbb{R}^m$ is determined through equation (2.8). We also set maximum numbers of iterations for the algorithms, which will be specified later.

Testing molecules and environment. All the test molecules in this section are described by restricted or unrestricted Kohn-Sham DFT (see Appendix A); basis sets and exchange-correlation functionals in use will be detailed later. The molecular geometries used in Sections 4.1-4.3 can be found in the Computational Chemistry Comparison and Benchmark DataBase (CCCBDB) [33], whereas the geometry used in Section 4.4 is from [2]. All the experiments are performed on a workstation with two Intel(R) Xeon(R) Processors Gold 5317 (at 3.00GHz×12, 18M Cache) and 512GB of RAM under Ubuntu 20.04.6. The codes are implemented in Python 3.10.19 with PySCF 2.11.0 [55].

4.1 Parameter settings

In this subsection, we determine the default parameters for the proposed DASSP. We test DASSP on three molecules: CO_2, C_2H_6, and $C_6H_5OCH_3$, treated within restricted Kohn-Sham DFT in PySCF. All calculations employ the `sto-3g` atomic-orbital basis set [28] and the PBE exchange-correlation functional [50]; as such, we have $(n, p) = (15, 11)$ for CO_2, $(n, p) = (16, 9)$ for C_2H_6, and $(n, p) = (48, 29)$ for $C_6H_5OCH_3$. We impose $m = 3, 6, 9$ quadratic constraints on CO_2, C_2H_6, and $C_6H_5OCH_3$, respectively. For each molecule, the symmetric constraint matrices $\{W_j\}_{j=1}^m$ are generated independently from the Gaussian distribution, and the corresponding $\{b_j\}_{j=1}^m$ are defined using a randomly generated reference point to ensure feasibility.

The algorithm is initialized randomly in this subsection. Specifically, $X^{(0)} \in \mathrm{St}_p(\mathbb{R}^n)$ is generated as a random matrix from the Gaussian distribution followed by a QR decomposition, $Y^{(0)}$ is initialized as the projection of $X^{(0)}(X^{(0)})^\top$ onto the affine set $\mathcal{Y}$, and the initial multiplier is $\Lambda^{(0)} = 0$. For a fair comparison, the same initialization is used within each parameter sweep.

We tune four components of DASSP in the following order: the stepsize strategy in the Y-update (2.7), the damping parameter δ, the penalty parameter β, and the under-relaxation parameter τ. In each experiment, only one parameter is varied while keeping the others fixed.

[5] Available at https://github.com/pyscf/pyscf/blob/master/examples/1-advanced/033-constrained_dft.py.

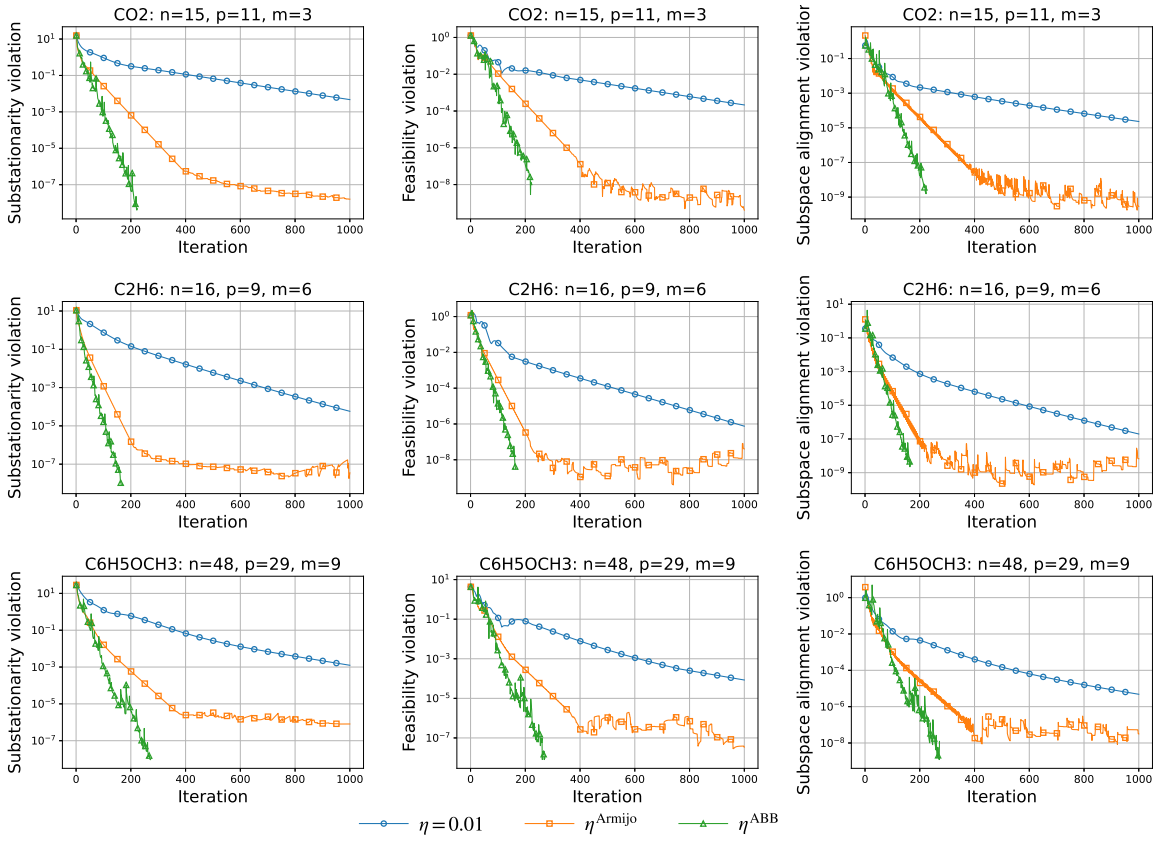

Figure 1: Comparison between different stepsize strategies. The blue curves with circle markers, orange curves with square markers, and green curves with triangle markers represent the results using the constant, Armijo backtracking, and clipped ABB strategies, respectively. From top to bottom: CO_2, C_2H_6, and $C_6H_5OCH_3$. From left to right: substationarity violation, feasibility violation, and subspace alignment violation.

Stepsize strategy. We fix $\beta = 20, \tau = 0.2$, and $\delta = 10^{-10}$ and compare three strategies for the projected gradient stepsize η_k in the Y-update (2.7): (1) constant stepsize[6].: $\eta_k \equiv 10^{-2}$; (2) Armijo backtracking line search: starting from $\eta_k = 10^{-2}$, the trial stepsize is halved until

$$\mathcal{L}_{\beta,\delta}(X^{(k+1)}, Y^{(k)} - \eta_k G^{(k)}, \Lambda^{(k)}) \le \mathcal{L}_{\beta,\delta}(X^{(k+1)}, Y^{(k)}, \Lambda^{(k)}) - 10^{-3} \cdot \eta_k \left\| G^{(k)} \right\|_{\mathrm{F}}^2$$

is satisfied; (3) clipped alternating Barzilai-Borwein (ABB) stepsize [13]:

$$\tilde{\eta}_k^{\mathrm{ABB}} := \begin{cases} 10^{-2}, & \text{if } k = 0, \\ \dfrac{\langle S^{(k-1)}, S^{(k-1)} \rangle}{|\langle S^{(k-1)}, Z^{(k-1)} \rangle|}, & \text{if } k \neq 0 \text{ is odd}, \\ \dfrac{|\langle S^{(k-1)}, Z^{(k-1)} \rangle|}{\langle Z^{(k-1)}, Z^{(k-1)} \rangle}, & \text{if } k \neq 0 \text{ is even}, \end{cases} \qquad \eta_k^{\mathrm{ABB}} := \min\{10, \max\{10^{-6}, \tilde{\eta}_k^{\mathrm{ABB}}\}\},$$

where $S^{(k-1)} := Y^{(k)} - Y^{(k-1)} \in \mathbb{S}^n$ and $Z^{(k-1)} := G^{(k)} - G^{(k-1)} \in \mathbb{S}^n$.

Figure 1 shows the results of DASSP with different strategies for η_k, where we also include the evolution of the subspace alignment violation, defined as $\|R^{(k)}\|_{\mathrm{F}}$ (see equation (3.1) and same below). Among the three strategies, the clipped ABB gives the most favorable overall performance. We therefore adopt $\eta_k = \eta_k^{\mathrm{ABB}}$ in all subsequent experiments.

[6]We note that this stepsize has been slightly tuned to improve the efficiency of the constant-stepsize strategy

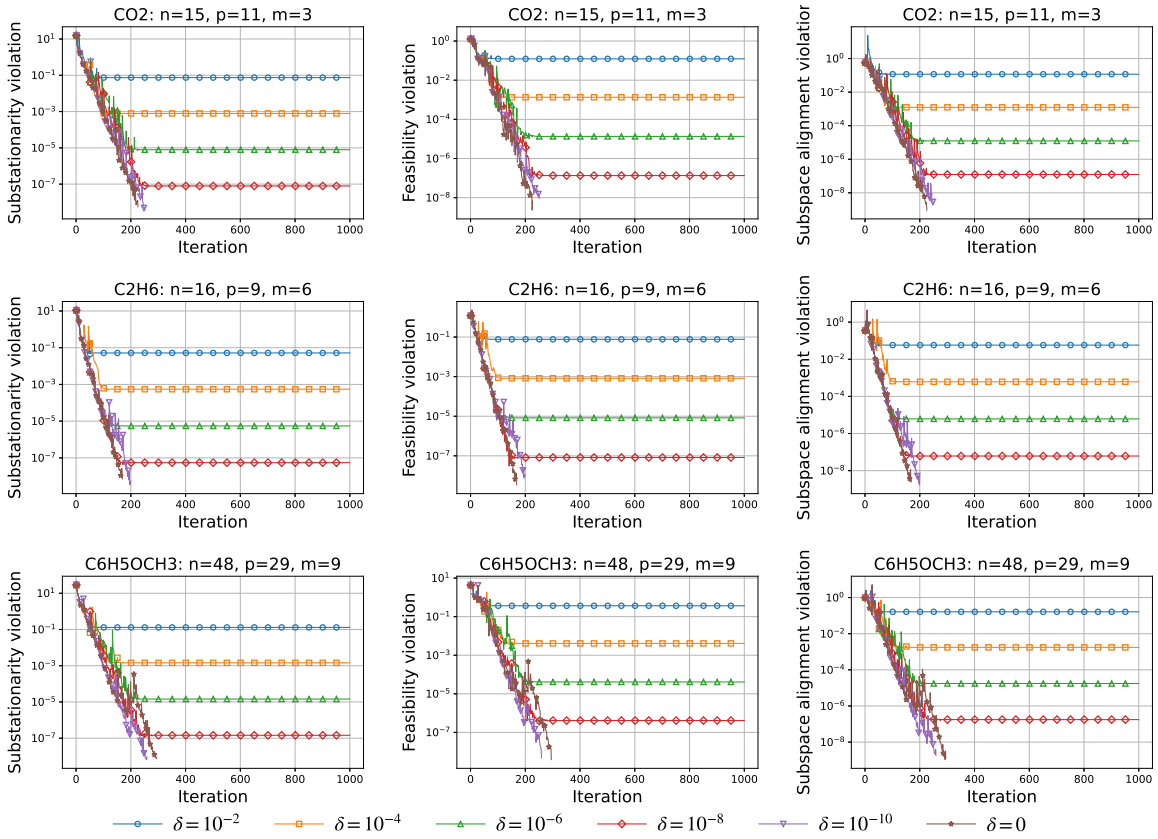

Figure 2: Comparison between different values of δ. The blue curves with circle markers, orange curves with square markers, green curves with triangle markers, red curves with diamond markers, purple curves with down-pointing triangle markers, and brown curves with star markers represent the results using $\delta = 10^{-2}, 10^{-4}, 10^{-6}, 10^{-8}, 10^{-10}, 0$, respectively. From top to bottom: CO_2, C_2H_6, and $C_6H_5OCH_3$. From left to right: substationarity violation, feasibility violation, and subspace alignment violation.

Damping parameter δ. We fix $\eta_k = \eta_k^{\mathrm{ABB}}, \beta = 20$, and $\tau = 0.2$, and vary the damping parameter over $\{10^{-2}, 10^{-4}, 10^{-6}, 10^{-8}, 10^{-10}, 0\}$. The numerical results are presented in Figure 2. For $\delta > 0$, we observe that DASSP produces an approximate KKT point and the accuracy is improved as δ decreases. This is consistent with Theorem 3.1. In particular, $\delta = 10^{-10}$ enables the algorithm to satisfy the stopping criterion in all tests. We also find that the choice $\delta = 0$, i.e., dual update without damping, leads to convergence across the board. Since the convergence curves of $\delta = 10^{-10}$ and $\delta = 0$ are nearly indistinguishable in our tests and using full dual updates is potentially more advantageous for efficiency, we adopt the choice $\delta = 0$ for ensuing experiments, even though its convergence is not covered in this work.

Penalty parameter β. We fix $\eta_k = \eta_k^{\mathrm{ABB}}$, $\delta = 0$, and $\tau = 0.2$ and vary the penalty parameter β within $\{5, 10, 20, 30, 40, 50, 100\}$. The numerical results are collected in Figure 3. We observe that DASSP manages to converge even when β is chosen as small as five, while its convergence behavior is strongly dependent on the value of β. Across the considered tests, the choice $\beta = 20$ achieves the best overall performance. The efficiency is significantly hindered if β is chosen to be either too small or too large relative to 20. Subsequently, we choose $\beta = 20$ as the default value.

Under-relaxation parameter τ. We fix $\eta_k = \eta_k^{\mathrm{ABB}}, \beta = 20$ and $\delta = 0$ and vary τ within $\{0.1, 0.2, \ldots, 0.8\}$. The numerical results are reported in Figure 4. We clearly observe that

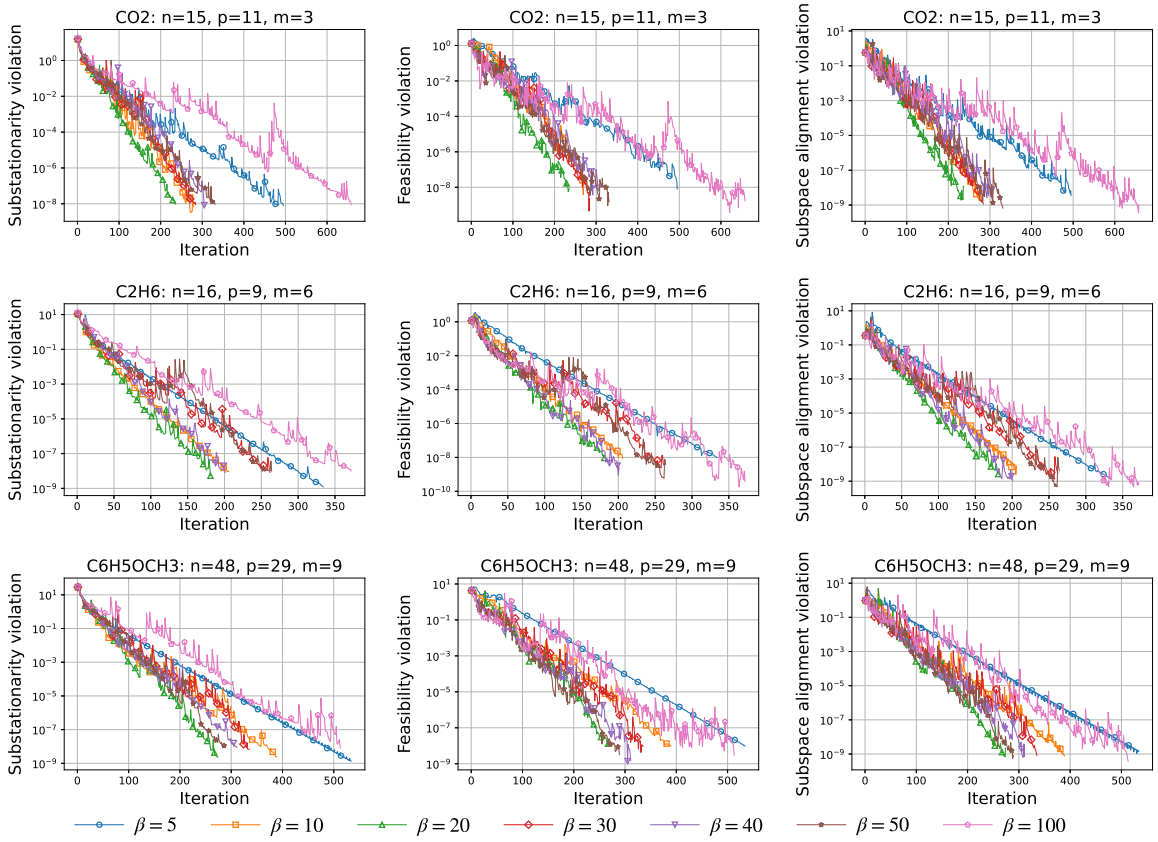

Figure 3: Comparison between different values of β. The blue curves with circle markers, orange curves with square markers, green curves with triangle markers, red curves with diamond markers, purple curves with down-pointing triangle markers, brown curves with star markers, and pink curves with pentagon markers represent the results using $\beta = 5, 10, 20, 30, 40, 50, 100$, respectively. From top to bottom: CO_2, C_2H_6, and $C_6H_5OCH_3$. From left to right: substationarity violation, feasibility violation, and subspace alignment violation.

values in the range $[0.1, 0.5]$ lead to much steadier convergence, with $\tau = 0.2$ and $\tau = 0.3$ the best two, in comparison with larger values. This indicates that the algorithm requires sufficient under-relaxation in dual updates to handle the nonlinear subspace alignment constraint. In the following, we set $\tau = 0.2$ as default.

These results lead to our default setting $(\eta_k, \beta, \delta, \tau) = (\eta_k^{\mathrm{ABB}}, 20, 0, 0.2)$ in DASSP. These default parameters will be used in the remaining experiments unless otherwise stated. We remark that these choices are not guaranteed to be optimal; the parameter tuning is not comprehensive in terms of both testing instances and tuning strategy. An adaptive way to choose these parameters would be preferable and will be studied in the future.

4.2 Effectiveness in handling nonconvex quadratic constraints

In this subsection, we demonstrate the effectiveness of DASSP in dealing with the nonconvex quadratic constraints through the numerical comparison with the QP-SCF, QP-PCAL, and WV methods. The experiments are conducted on an HCN molecule under a charge-transfer process. We describe the molecule by restricted Kohn-Sham DFT, adopting the `sto-3g` atomic-orbital basis set [28] and the PBE exchange-correlation functional [50]; therefore, we have $(n, p) = (22, 7)$. The charge-transfer process is imposed on the localized populations of the C $2p$ and N $2p$

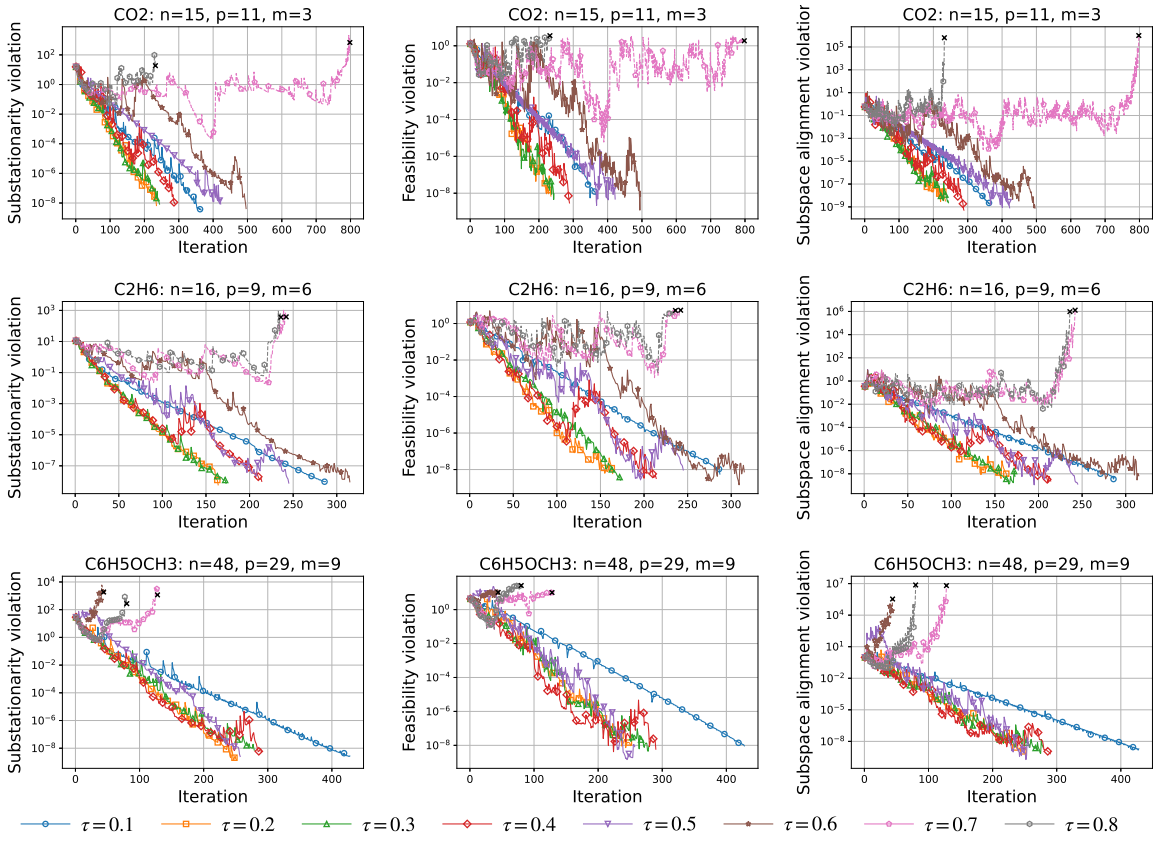

Figure 4: Comparison between different values of τ. The blue curves with circle markers, orange curves with square markers, green curves with triangle markers, red curves with diamond markers, purple curves with down-pointing triangle markers, brown curves with star markers, pink curves with pentagon markers, and gray curves with hexagon markers represent the results using $\tau = 0.1, 0.2, \ldots, 0.8$, respectively. From top to bottom: CO_2, C_2H_6, and $C_6H_5OCH_3$. From left to right: substationarity violation, feasibility violation, and subspace alignment violation.

subspaces with the shift amount $s = 0.5$; hence, $m = 2$. The construction of nonconvex quadratic constraints associated with the charge transfer is detailed in Appendix B. All methods are initialized from the `minao` guess provided by PySCF [3, 57]; for DASSP, we further set $\Lambda^{(0)} = 0$. The penalty parameter σ in the QP-SCF and QP-PCAL is varied within $\{1, 10, 100, 1000\}$. The maximum (outer-loop) iteration number for both QP-SCF and WV methods is set to 500.

The numerical results are reported in Table 1. The QP-PCAL (with any σ), WV, and DASSP are all found to converge, while the QP-SCF only works with $\sigma = 1$. When using a larger σ, the QP-SCF suffers from severe oscillations in the SCF iteration, as shown by the energy curves in Figure 5. This instability can be understood from the fixed-point viewpoint of the SCF iteration. As shown in [46], the Jacobian of the SCF fixed-point map depends on the derivative of the effective Hamiltonian. For the QP-SCF, such a derivative contains an additional term proportional to σ. A large penalty parameter σ could then enlarge the norm of the Jacobian of the SCF map, thereby spoiling the local contractivity of the SCF iteration.

In contrast to QP-SCF, the QP-PCAL converges robustly regardless of σ. Nevertheless, it terminates at infeasible solutions with respect to the nonconvex quadratic constraints, even with $\sigma = 1000$. The results in Table 1 also suggest that we could improve its final feasibility violation by further increasing the value of σ, yet at the price of using more computational resources due to the worse conditioning. As PCAL is observed to converge, we could infer from such deficiency

Table 1: Comparison between QP-SCF, QP-PCAL, WV, and DASSP on the HCN charge-transfer test. The final energies, feasibility violations (Feas.), numbers of iterations (Iter.) and wall-clock times are listed. For the WV method, the values outside and inside the parentheses refer to the outer iteration numbers and the averaged inner iteration numbers, respectively.

Algorithm	Energy (E_h)	Iter.	Feas.	Time (s)
QP-SCF ($\sigma = 1$)	−9.203372001e+01	71	8.286e−02	3.14
QP-SCF ($\sigma = 10$)	−8.172849033e+01	500	2.917e+00	21.24
QP-SCF ($\sigma = 100$)	−8.627036448e+01	500	2.917e+00	20.98
QP-SCF ($\sigma = 1000$)	−8.213467723e+01	500	2.917e+00	29.00
QP-PCAL ($\sigma = 1$)	−9.203372001e+01	199	8.286e−02	2.84
QP-PCAL ($\sigma = 10$)	−9.201331705e+01	302	1.052e−02	4.30
QP-PCAL ($\sigma = 100$)	−9.201061596e+01	805	1.087e−03	11.42
QP-PCAL ($\sigma = 1000$)	−9.201033596e+01	2085	1.091e−04	29.58
WV	−9.201030473e+01	85(8.53)	7.303e−09	13.68
DASSP	−9.201030473e+01	293	3.685e−09	3.08

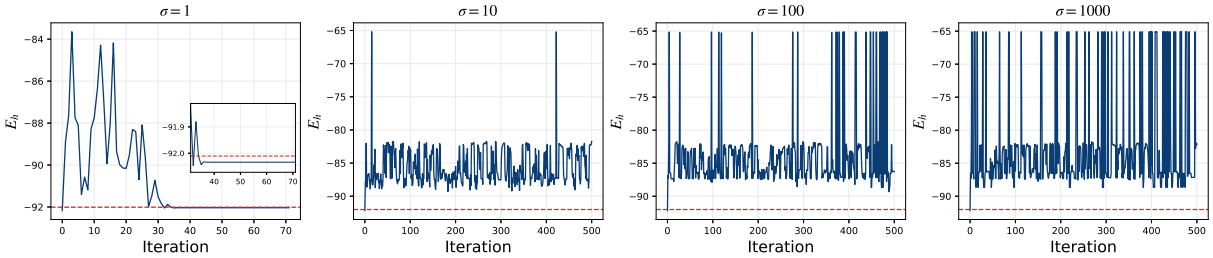

Figure 5: Energy curves of the QP-SCF with different values of σ. The red dashed line represents the energy obtained by DASSP.

of the QP-PCAL that the quadratic penalty function (1.3) is likely not exact for the nonlinear quadratic constraints in problem (1.2).

Compared with QP-SCF and QP-PCAL, the WV and DASSP are free from the issues related to quadratic penalty and are effective in dealing with the nonlinear quadratic constraints. In particular, the proposed DASSP reformulates these constraints into linear ones by introducing an extra variable Y, and ensures the feasibility of Y via closed-form projections. The discrepancy between X and Y is handled within an augmented Lagrangian framework, which does not require an excessively large penalty parameter. In the following experiments, we focus on the comparison between the proposed DASSP and the WV method.

4.3 Comparison of computational efficiency

In this subsection, we compare the efficiency of the proposed DASSP and the WV method on a series of charge-transfer tests. We consider three molecular systems, HCN, C_2H_4, and CH_3COCH_3, described at the same level of theory as in Section 4.2. For HCN, $(n, p) = (22, 7)$ and the transfer is imposed between the C $2p$ and N $2p$ orbitals; for C_2H_4, $(n, p) = (28, 8)$ and the transfer is imposed between the 2p orbitals on the two carbon atoms; for CH_3COCH_3, $(n, p) = (52, 16)$ and the transfer is imposed between the $2p$ orbitals associated with the C and O atoms of the carbonyl group. Hence, we have $m = 2$ for all the tests in this subsection. The shift amount s is varied within $\{0.2, 0.4, 0.6, 0.8, 1.0\}$. Both the WV method and DASSP are initialized from the `minao` guess provided by PySCF; for DASSP, we further set $\Lambda^{(0)} = 0$. The maximum number of outer iterations in the WV method is set to 500.

Table 2: Comparison between DASSP and WV method on charge-transfer tests under different shift amounts s. The final energies, feasibility violations (Feas.), numbers of iterations (Iter.) and wall-clock times are listed. For the WV method, the values outside and inside the parentheses refer to the outer iteration numbers and the averaged inner iteration numbers, respectively.

HCN system: $n = 22,\ p = 7$					
s	Algorithm	Energy (E_h)	Iter.	Feas.	Time (s)
0.2	WV	−9.208154276e+01	41(14.27)	5.791e−09	9.06
	DASSP	−9.208154275e+01	261	2.838e−09	2.75
0.4	WV	−9.204088277e+01	71(10.34)	4.313e−09	12.14
	DASSP	−9.204088276e+01	232	1.075e−09	2.52
0.6	WV	−9.197283505e+01	102(7.74)	7.026e−09	13.90
	DASSP	−9.197283504e+01	280	2.049e−09	1.87
0.8	WV	−9.187696735e+01	76(8.17)	5.660e−09	10.71
	DASSP	−9.187696736e+01	303	5.862e−10	2.05
1.0	WV	−9.175261870e+01	19(23.84)	1.662e−09	4.87
	DASSP	−9.175261870e+01	332	8.110e−10	3.29
C_2H_4 system: $n = 28,\ p = 8$					
s	Algorithm	Energy (E_h)	Iter.	Feas.	Time (s)
0.2	WV	−7.749661121e+01	19(19.47)	3.883e−09	9.97
	DASSP	−7.749661123e+01	340	4.743e−09	4.91
0.4	WV	−7.746190903e+01	19(18.89)	3.750e−09	9.54
	DASSP	−7.746190902e+01	493	6.683e−09	7.25
0.6	WV	−7.740360110e+01	19(21.21)	4.508e−09	10.65
	DASSP	−7.740360108e+01	364	7.581e−09	5.32
0.8	WV	−7.732089387e+01	19(19.21)	7.192e−09	9.78
	DASSP	−7.732089389e+01	536	1.256e−09	7.95
1.0	WV	−7.721248200e+01	19(18.53)	5.354e−09	9.33
	DASSP	−7.721248200e+01	494	2.345e−10	7.34
CH_3COCH_3 system: $n = 52,\ p = 16$					
s	Algorithm	Energy (E_h)	Iter.	Feas.	Time (s)
0.2	WV	−1.903782768e+02	17(20.24)	1.141e−09	21.84
	DASSP	−1.903782767e+02	354	3.418e−09	18.29
0.4	WV	−1.903295420e+02	112(6.29)	6.302e−09	57.17
	DASSP	−1.903295420e+02	372	5.223e−09	18.61
0.6	WV	−1.902483369e+02	39(12.41)	5.329e−09	32.64
	DASSP	−1.902483368e+02	332	4.926e−10	16.89
0.8	WV	−1.901343269e+02	235(3.78)	7.396e−09	80.03
	DASSP	−1.901343270e+02	348	1.401e−10	17.42
1.0	WV	−1.899868593e+02	101(5.42)	5.848e−10	43.51
	DASSP	−1.899868593e+02	283	1.927e−09	13.81

The numerical results are summarized in Table 2. For all the tests here, both methods converge and attain essentially the same energies with comparable feasibility violations. For C_2H_4, the efficiency of DASSP is slightly better than that of the WV method. But for both HCN and CH_3COCH_3, DASSP is found to yield prominent accelerations. Such superiority could be credited to the single-loop nature of DASSP. In contrast, although the WV method may require only a few outer iterations, its efficiency depends heavily on the inner dual Newton

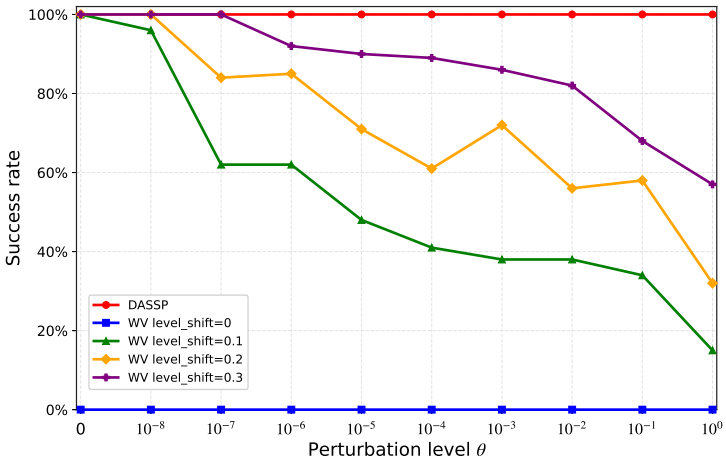

Figure 6: Success rates of DASSP and WV methods as functions of the perturbation level on the $(H_2O)_2{}^+$ charge-localization test. The red curve with circle markers represents the results of DASSP, while the blue curve with square markers, green curve with triangle markers, yellow curve with diamond markers, and purple curve with plus sign markers represent those of the WV method with a level shift of 0, 0.1, 0.2, and 0.3, respectively.

steps.

4.4 Comparison of robustness

In this subsection, we aim to numerically showcase the robustness advantage of DASSP over the WV method. We consider a representative charge-localization benchmark for CDFT, the water dimer cation $(H_2O)_2{}^+$ in vacuum, following the setup in [2]. The two water molecules are separated by a center-of-mass distance of 10 Å. We describe the system under unrestricted Kohn-Sham DFT, using the PBE exchange-correlation functional [50] with the D3 dispersion correction [24] and the `def2-svp` basis set [60], for which we have $(n, p) = (96, 19)$. The charge-localization constraint ($m = 1$) is imposed between two water fragments, based on the Hirshfeld charge partitioning scheme; please refer to Appendix B for details.

We initialize both methods at random perturbations of a reference solution and compare their robustness using success rates as functions of the perturbation level. We first compute the reference solution by running DASSP with a tolerance of 10^{-8} and denote the final splitting variable by $Y_{\text{ref}} \in \mathbb{S}^n$. For any perturbation level $\theta > 0$, the initial point for both DASSP and WV methods is generated as $Y^{(0)} := Y_{\text{ref}} + \theta N$, where $N \in \mathbb{S}^n$ is a symmetric random matrix sampled from the Gaussian distribution. We vary the perturbation level θ within $\{0, 10^{-8}, 10^{-7}, 10^{-6}, 10^{-5}, 10^{-4}, 10^{-3}, 10^{-2}, 10^{-1}, 1\}$; for each value of θ, 100 independent trials are conducted using both methods. Throughout the tests in this subsection, we set $\Lambda^{(0)} = 0$ for DASSP and $\boldsymbol{\mu}^{(0)} = 0$ for the WV method. The maximum number of outer loops in the WV method is set to 500.

The numerical results are reported in Figure 6, where the red and blue curves denote DASSP and the plain WV method, respectively. The proposed DASSP is found to yield success rates of 100% across the considered perturbation levels on this example. In sharp contrast, the plain WV method fails in all tests without any exception; in particular, it does not work even when the initialization is taken directly from the reference solution. As discussed in Section 1, the convergence of the WV method could be problematic when the eigengap of the effective Hamiltonian is tiny. Therefore, we evaluate the eigengap of $F(X_{\text{ref}}, \mu_{\text{ref}})$ at the reference solution, where $X_{\text{ref}} \in \text{St}_p(\mathbb{R}^n)$ satisfies $X_{\text{ref}} X_{\text{ref}}^\top = Y_{\text{ref}}$ and μ_{ref} is obtained by solving the linear system

(2.8). The eigengap turns out to be extremely small, approximately 1.103×10^{-12}.

Intuitively, with such a tiny eigengap, the outer loop of the WV method can be unstable in selecting the lowest p eigenvectors. Worse still, a tiny eigengap is also harmful to the inner Newton steps, as the required Jacobian relies on its reciprocal [61]. We corroborate these explanations by monitoring the eigengap and consecutive subspace distance, $\|X^{(k)}(X^{(k)})^\top - X^{(k+1)}(X^{(k+1)})^\top\|_{\mathrm{F}}$, of the WV method, using either random initialization with a perturbation level of $\theta = 10^{-8}$ described above or the `minao` guess provided by PySCF (whose distance from the reference solution is 1.649). We collect the results in Figure 7. Under both initializations, the eigengap of the effective Hamiltonian fluctuates severely over the outer iterations and becomes small from time to time, and the subspace distance exhibits persistent oscillations. These observations indicate that the WV method fails to stabilize subspaces, even when the initial point is already sufficiently close to the reference solution.

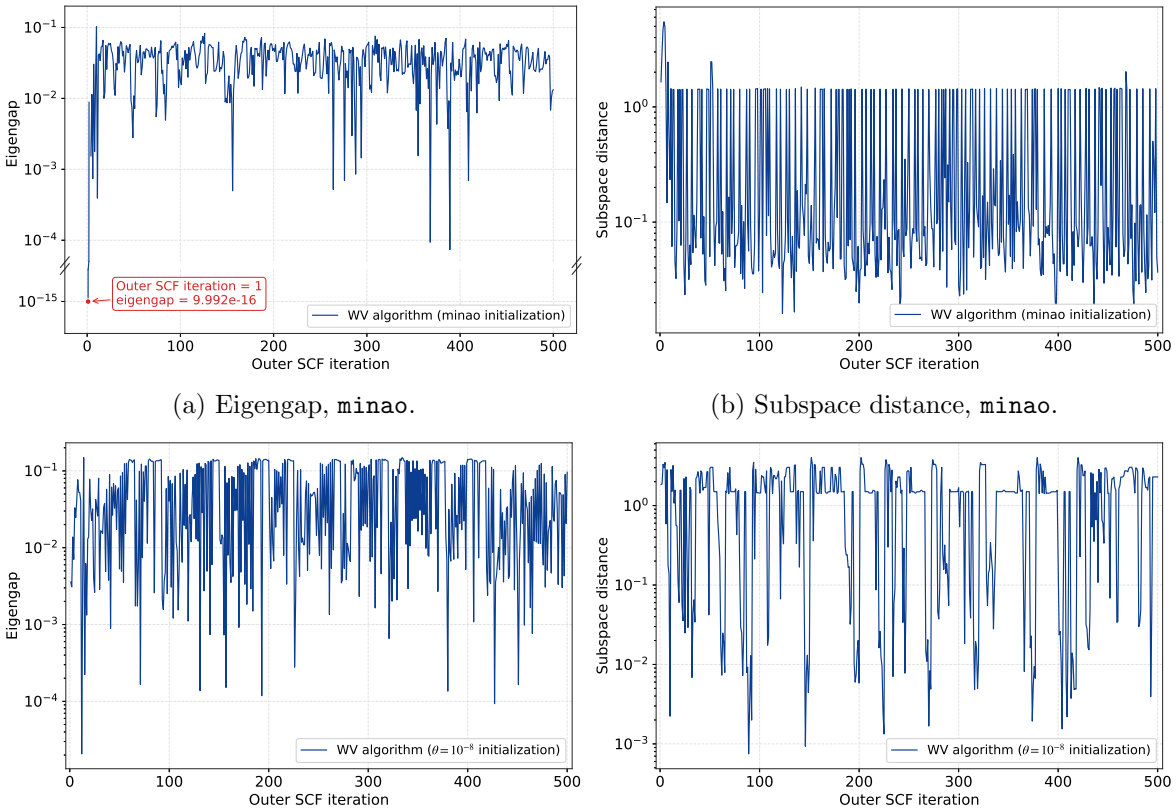

(a) Eigengap, `minao`.

(b) Subspace distance, `minao`.

(c) Eigengap, random.

(d) Subspace distance, random.

Figure 7: Evolutions of the eigengap of the effective Hamiltonian and consecutive subspace distance of the WV algorithm with either `minao` guess (panels (a) and (b)) or randomly perturbed initialization (panels (c) and (d)).

We acknowledge that the convergence proof of DASSP also involves an eigengap-type Assumption 3.1 (A2) on the matrix $A^{(k)}$ in the X-subproblem (2.4), which is not the same as the effective Hamiltonian in the WV method. Although we cannot remove this assumption in the current analysis, we present here a numerical investigation. To stay in line with the convergence analysis in Section 3, we consider DASSP using $\delta = 10^{-10}$, starting with random initialization with a perturbation level of $\theta = 1$ or the `minao` guess by PySCF. The numerical results are presented in Figure 8. These plots show that the eigengap of $A^{(k)}$ quickly rises to a positive plateau and remains bounded away from zero, even though the initial eigengap of $A^{(0)}$ may vanish (see panel (a) in Figure 8). This suggests that Assumption 3.1 (A2) is not restrictive in practice. By

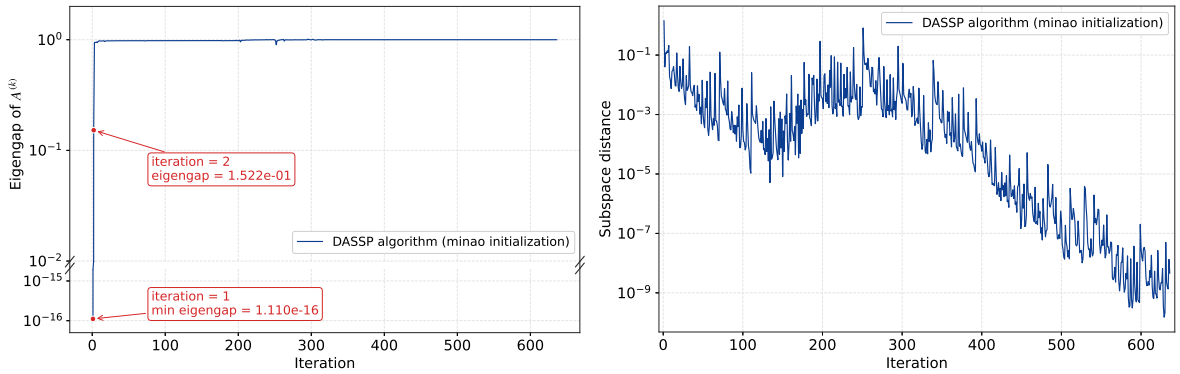

(a) Eigengap, `minao`.

(b) Subspace distance, `minao`.

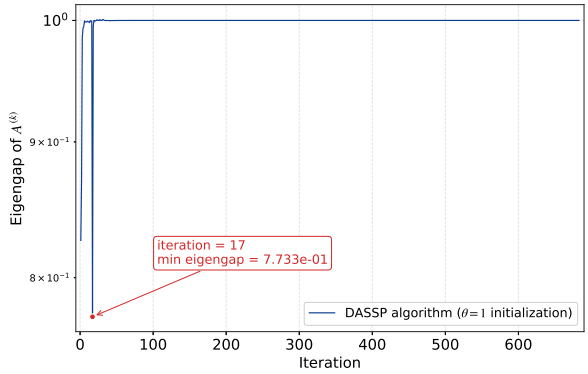

(c) Eigengap, random.

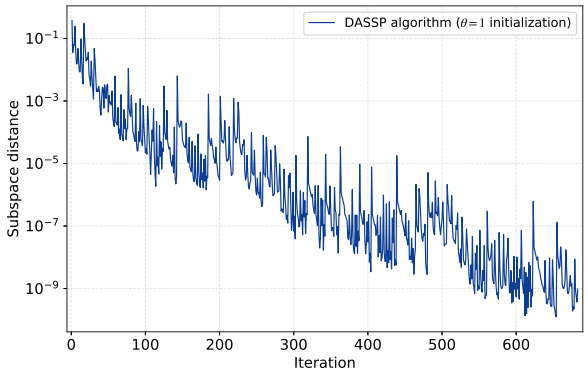

(d) Subspace distance, random.

Figure 8: Evolutions of the eigengap of the matrix $A^{(k)}$ and consecutive subspace distance of DASSP with either `minao` guess (panels (a) and (b)) or randomly perturbed initialization (panels (c) and (d)).

virtue of the behavior shown in Figure 8, DASSP converges steadily to the reference solution.

In the SCF literature (e.g., [4]), a commonly used strategy to mitigate the issues related to small eigengap is to introduce a level shift into the effective Hamiltonian, which artificially enlarges the eigengap between the p-th and $(p+1)$-th smallest eigenvalues and may improve the stability of the SCF iteration. In PySCF, this can be achieved by setting the tag `level_shift`. We also test the WV method with the amount of level shift within $\{0.1, 0.2, 0.3\}$, under the same perturbed initialization strategy above. The success rates are also shown in Figure 6. One can see that level shifting indeed improves the robustness of the WV method, and as the amount of level shift increases, the success rate is getting better. Nevertheless, the success rate of the WV method still exhibits a clear decreasing trend as the perturbation level grows. In addition, as pointed out in [4], increasing the amount of level shift would degrade the efficiency of the algorithm. In comparison, DASSP offers both efficiency and robustness under the default parameter setting.

5 Conclusions

In this paper, we study the optimization problem arising from CDFT. Compared with that for ground-state DFT calculations, it is more challenging due to the presence of both the Stiefel manifold and nonconvex quadratic constraints. By exploiting the inherent rotation invariance, we decouple the two groups of constraints by introducing an additional nonlinear subspace alignment constraint. For the reformulated problem, we propose a single-loop damped ADMM

termed DASSP, which, to the best of our knowledge, is the first algorithm with rigorous convergence guarantees for CDFT calculations. Each iteration of DASSP consists of a spectral minimization step, a projected-gradient step, and a damped dual update. Numerical tests have been conducted on synthetic and realistic charge-transfer and charge-localization CDFT calculations. The obtained results demonstrate that DASSP is effective in dealing with the nonconvex quadratic constraints, and exhibits comparable performance or substantial acceleration over state-of-the-art methods without compromising robustness.

Several directions merit further investigation. First, it is of theoretical interest to the broader ADMM community to study the convergence properties in the undamped case ($\delta = 0$). Our numerical results show that the undamped version converges steadily and is efficient, while the analysis in this paper only applies to the damped regime ($\delta > 0$). Second, it is preferable to investigate an adaptive way to choose the parameters in DASSP for general settings. Third, it would be practically meaningful to apply or adapt DASSP to other CDFT settings. For example, in noncollinear calculations, one could impose constraints on local atomic magnetic moments to study the potential energy surfaces of magnetic materials. The underlying problems may involve larger numbers of nonconvex quadratic constraints than the considered charge-transfer or charge-localization problems considered here. We could thus anticipate a more prominent advantage of DASSP over the double-loop method, which relies on a dual scheme for inner iterations. Finally, it is promising to integrate DASSP for first-principles calculations into machine-learning-assisted quantum chemistry and quantum physics workflows. For challenging applications such as magnetic materials and charge-transfer processes, large, high-quality first-principles datasets are essential but remain scarce. The efficiency and robustness of DASSP suggest its potential for generating high-quality CDFT datasets in such settings.

A Discretized formulation of CDFT

We describe how the continuous CDFT formulation (1.1) is discretized into the finite-dimensional optimization model (1.2) used throughout the paper. For simplicity, we take restricted Kohn-Sham DFT (RKS-DFT) in closed-shell collinear calculations as an example.

In collinear calculations, spinor orbitals are assumed to be of the form $\psi_i = (\varphi_i, 0)^\top$ (spin-up) or $\psi_i = (0, \varphi_i)^\top$ (spin-down), where φ_i is a spatial orbital. Within RKS-DFT, each spatial orbital is doubly occupied by electrons of opposite spin with identical spatial functions. Let $\{\chi_\mu\}_{\mu=1}^{n_\mathrm{b}}$ be a set of real atomic-orbitals, where $n_\mathrm{b} \in \mathbb{N}$ denotes the number of basis functions. For brevity, we assume here (and in Appendix B) that the atomic orbitals are orthonormal in the L^2 inner product (which can be enforced using the Löwdin transformation). The spatial orbital is expressed as a linear combination of atomic orbitals:

$$\varphi_i = \sum_{\mu=1}^{n_\mathrm{b}} X_{\mu i}\chi_\mu, \quad i = 1, \ldots, N_\mathrm{o} \quad \text{with} \quad N_\mathrm{o} := N/2.$$

Here, N_o denotes the number of occupied spatial orbitals and $X \in \mathbb{R}^{n_\mathrm{b}\times N_\mathrm{o}}$ denotes the orbital coefficient matrix. The orthonormality condition on the spinor orbitals then reduces to the constraint $X^\top X = I_{N_\mathrm{o}}$ on X. The reduced one-body density matrix is defined as $Y := XX^\top \in \mathbb{S}^{n_\mathrm{b}}$. The spin densities are thus given by

$$\rho^{\uparrow,\uparrow}(\boldsymbol{r}) = \rho^{\downarrow,\downarrow}(\boldsymbol{r}) = \sum_{1\le\mu,\nu\le n_\mathrm{b}} Y_{\mu\nu}\chi_\mu(\boldsymbol{r})\chi_\nu(\boldsymbol{r}) \quad \text{and} \quad \rho^{\uparrow,\downarrow} = \rho^{\downarrow,\uparrow} \equiv 0. \tag{A.1}$$

In the chosen atomic-orbital basis, the discretized RKS-DFT energy functional is

$$f(Y) = 2\mathrm{Tr}(hY) + 2\mathrm{Tr}(J(Y)Y) + E_\mathrm{xc}(Y) + E_\mathrm{nn},$$

where $h = [h_{\mu\nu}] \in \mathbb{S}^{n_\mathrm{b}}$ is the discretized one-body Hamiltonian,

$$h_{\mu\nu} := \int_{\mathbb{R}^3} \chi_\mu(\boldsymbol{r}) \left(-\frac{1}{2}\Delta + V_{\mathrm{ext}}(\boldsymbol{r}) \right) \chi_\nu(\boldsymbol{r}) \, \mathrm{d}\boldsymbol{r}, \quad 1 \le \mu, \nu \le n_\mathrm{b},$$

with V_{ext} the external potential (e.g., induced by nuclei), $J : \mathbb{S}^{n_\mathrm{b}} \to \mathbb{S}^{n_\mathrm{b}}$ is the self-adjoint Coulomb operator, defined as

$$[J(Y)]_{\mu\nu} := \sum_{1 \le \sigma, \tau \le n_\mathrm{b}} g_{\mu\nu\sigma\tau} Y_{\sigma\tau}, \quad 1 \le \mu, \nu \le n_\mathrm{b},$$

with the two-body integrals

$$g_{\mu\nu\sigma\tau} := \int_{\mathbb{R}^3} \int_{\mathbb{R}^3} \frac{\chi_\mu(\boldsymbol{r}) \chi_\nu(\boldsymbol{r}) \chi_\sigma(\boldsymbol{r}') \chi_\tau(\boldsymbol{r}')}{\|\boldsymbol{r} - \boldsymbol{r}'\|} \, \mathrm{d}\boldsymbol{r} \, \mathrm{d}\boldsymbol{r}', \quad 1 \le \mu, \nu, \sigma, \tau \le n_\mathrm{b},$$

$E_{\mathrm{xc}} : \mathbb{S}^{n_\mathrm{b}} \to \mathbb{R}$ is the exchange-correlation functional, and E_{nn} is the nuclear repulsion term.

In the chosen atomic-orbital basis, equation (A.1) implies that the additional density constraints in CDFT can be discretized into the form $\mathrm{Tr}(X^\top W_j X) = b_j$, where in particular

$$[W_j]_{\mu\nu} = \int_{\mathbb{R}^3} \chi_\mu(\boldsymbol{r}) \big(w_j^{\uparrow,\uparrow}(\boldsymbol{r}) + w_j^{\downarrow,\downarrow}(\boldsymbol{r}) \big) \chi_\nu(\boldsymbol{r}) \, \mathrm{d}\boldsymbol{r}, \quad 1 \le \mu, \nu \le n_\mathrm{b}. \tag{A.2}$$

In summary, the finite-dimensional discretization of the CDFT problem (1.1) within RKS-DFT takes the form (1.2) with $n = n_\mathrm{b}$ and $p = N_\mathrm{o}$. We remark that the extensions to the unrestricted case (UKS-DFT) and noncollinear case are straightforward. In UKS-DFT, the spatial orbitals in the spin-up and spin-down channels are independently optimized and may differ. In the noncollinear case, both components of the spinor orbitals are nonzero and no fixed global spin quantization axis exists.

B Construction of nonconvex quadratic constraints

Charge-transfer problems. This construction is used in the experiments in Sections 4.2 and 4.3. Following standard population analysis in CDFT, fragment charges are measured in a localized-orbital basis. Let $C_{\mathrm{loc}} \in \mathbb{R}^{n_\mathrm{b} \times n_\mathrm{b}}$ denote the localized-orbital transformation satisfying $C_{\mathrm{loc}}^\top C_{\mathrm{loc}} = I_{n_\mathrm{b}}$, which can be constructed by the meta-Löwdin orthogonalization routine in PySCF. Let $\mathcal{I}_A$ and $\mathcal{I}_B$ denote the sets of localized orbitals associated with fragments A and B, respectively. We define the corresponding population matrices by

$$W_A := \sum_{\ell \in \mathcal{I}_A} c_\ell c_\ell^\top \in \mathbb{S}^{n_\mathrm{b}}, \qquad W_B := \sum_{\ell \in \mathcal{I}_B} c_\ell c_\ell^\top \in \mathbb{S}^{n_\mathrm{b}},$$

where $c_\ell \in \mathbb{R}^{n_\mathrm{b}}$ is the ℓ-th column of C_{loc}. Let $X_{\mathrm{ref}} \in \mathbb{R}^{n \times p}$ be a reference solution obtained from, e.g., a ground-state DFT calculation and let $s > 0$ denote the prescribed charge-transfer amount. Then we impose the charge-transfer constraints as follows:

$$\mathrm{Tr}(X^\top W_A X) = b_A := \mathrm{Tr}(X_{\mathrm{ref}}^\top W_A X_{\mathrm{ref}}) + s, \quad \mathrm{Tr}(X^\top W_B X) = b_B := \mathrm{Tr}(X_{\mathrm{ref}}^\top W_B X_{\mathrm{ref}}) - s.$$

That is, we enforce a charge transfer of size s from fragment B to fragment A.

Charge-localization problems. This applies to the experiments in Section 4.4. Let L and R denote the two water fragments, corresponding to the left and right molecules, respectively. For each atom a, let ρ_a^0 be the promolecular atomic density centered at the nuclear position $\boldsymbol{R}_a \in \mathbb{R}^3$, obtained from a DFT calculation with atom a in isolation. In our implementations, we use the

same exchange-correlation functional and basis set for all atoms. The Hirshfeld weight function is then defined by

$$w(\boldsymbol{r}) := \frac{\sum_{a\in L} \rho_a^0(\boldsymbol{r}-\boldsymbol{R}_a) - \sum_{a\in R} \rho_a^0(\boldsymbol{r}-\boldsymbol{R}_a)}{\sum_a \rho_a^0(\boldsymbol{r}-\boldsymbol{R}_a)}.$$

Here, the denominator is the total promolecular density. Following the standard Hirshfeld implementation [2], when this denominator is smaller than 10^{-12}, we set $w(\boldsymbol{r}) = 0$ for numerical stability. The Hirshfeld charge constraint takes the form $\mathrm{Tr}(X^\top W X) = N_c$, where the matrix W is defined as in equation (A.2) with $w^{\uparrow,\uparrow} = w^{\downarrow,\downarrow} = w$. For the water dimer cation, we set $N_c = 1$, which corresponds to a one-electron charge-difference constraint between the two water fragments.

References

[1] P.-A. Absil, R. Mahony, and R. Sepulchre. *Optimization Algorithms on Matrix Manifolds*. Princeton University Press, 2008.

[2] C. S. Ahart, K. M. Rosso, and J. Blumberger. Implementation and validation of constrained density functional theory forces in the CP2K package. *J. Chem. Theory Comput.*, 18(7):4438–4446, 2022.

[3] J. Almlöf, K. Fægri Jr, and K. Korsell. Principles for a direct SCF approach to LICAO-MO*ab-initio* calculations. *J. Comput. Chem.*, 3(3):385–399, 1982.

[4] Z. Bai, R.-C. Li, and D. Lu. Sharp estimation of convergence rate for self-consistent field iteration to solve eigenvector-dependent nonlinear eigenvalue problems. *SIAM J. Matrix Anal. Appl.*, 43(1):301–327, 2022.

[5] V. Balzani, P. Ceroni, and A. Juris. *Photochemistry and Photophysics: Concepts, Research, Applications*. John Wiley & Sons, 2014.

[6] R. Bergmann and R. Herzog. Intrinsic formulation of KKT conditions and constraint qualifications on smooth manifolds. *SIAM J. Optim.*, 29(4):2423–2444, 2019.

[7] J. Bolte, S. Sabach, and M. Teboulle. Nonconvex Lagrangian-based optimization: monitoring schemes and global convergence. *Math. Oper. Res.*, 43(4):1210–1232, 2018.

[8] S. Boyd, N. Parikh, E. Chu, B. Peleato, and J. Eckstein. Distributed optimization and statistical learning via the alternating direction method of multipliers. *Found. Trends Mach. Learn.*, 3(1):1–122, 2011.

[9] K. Burke. Perspective on density functional theory. *J. Chem. Phys.*, 136(15), 2012.

[10] Z. Cai, K. Wang, Y. Xu, S.-H. Wei, and B. Xu. A self-adaptive first-principles approach for magnetic excited states. *Quantum Front.*, 2(1):21, 2023.

[11] E. Cancès and G. Friesecke. *Density Functional Theory: Modeling, Mathematical Analysis, Computational Methods, and Applications*. Mathematics and Molecular Modeling. Springer Cham, 2023.

[12] E. Cohen, N. Hallak, and M. Teboulle. A dynamic alternating direction of multipliers for nonconvex minimization with nonlinear functional equality constraints. *J. Optim. Theory Appl.*, 193(1):324–353, 2022.

[13] Y.-H. Dai and R. Fletcher. Projected Barzilai-Borwein methods for large-scale box-constrained quadratic programming. *Numer. Math.*, 100(1):21–47, 2005.

[14] P. H. Dederichs, S. Blügel, R. Zeller, and H. Akai. Ground states of constrained systems: application to cerium impurities. *Phys. Rev. Lett.*, 53(26):2512, 1984.

[15] K. Deng, J. Jin, J. Hu, and H. Wang. Adaptive Riemannian ADMM for nonsmooth optimization: optimal complexity without smoothing. In *The 39th Conference on Neural Information Processing Systems*, 2025.

[16] L. El Bourkhissi and I. Necoara. Convergence rates for an inexact linearized ADMM for nonsmooth nonconvex optimization with nonlinear equality constraints. *Comput. Optim. Appl.*, pages 1–39, 2025.

[17] D. Gabay and B. Mercier. A dual algorithm for the solution of nonlinear variational problems via finite element approximation. *Comput. Math. Appl.*, 2(1):17–40, 1976.

[18] B. Gao, G. Hu, Y. Kuang, and X. Liu. An orthogonalization-free parallelizable framework for all-electron calculations in density functional theory. *SIAM J. Sci. Comput.*, 44(3):B723–B745, 2022.

[19] B. Gao, X. Liu, and Y.-X. Yuan. Parallelizable algorithms for optimization problems with orthogonality constraints. *SIAM J. Sci. Comput.*, 41(3):A1949–A1983, 2019.

[20] A. García, N. Papior, A. Akhtar, E. Artacho, V. Blum, E. Bosoni, P. Brandimarte, M. Brandbyge, J. I. Cerdá, F. Corsetti, R. Cuadrado, V. Dikan, J. Ferrer, J. Gale, P. García-Fernández, V. M. García-Suárez, S. García, G. Huhs, S. Illera, R. Korytár, P. Koval, I. Lebedeva, L. Lin, P. López-Tarifa, S. G. Mayo, S. Mohr, P. Ordejón, A. Postnikov, Y. Pouillon, M. Pruneda, R. Robles, D. Sánchez-Portal, J. M. Soler, R. Ullah, V. W.-Z. Yu, and J. Junquera. SIESTA: recent developments and applications. *J. Chem. Phys.*, 152(20):204108, 2020.

[21] R. Glowinski and A. Marroco. Sur l'approximation, par éléments finis d'ordre un, et la résolution, par pénalisation-dualité d'une classe de problèmes de Dirichlet non linéaires. *RAIRO. Anal. numér.*, 9(R2):41–76, 1975.

[22] G. H. Golub and C. F. Van Loan. *Matrix Computations*. Johns Hopkins University Press, 4th edition, 2013.

[23] X. Gonze, B. Seddon, J. A. Elliott, C. Tantardini, and A. V. Shapeev. Constrained density functional theory: a potential-based self-consistency approach. *J. Chem. Theory Comput.*, 18(10):6099–6110, 2022.

[24] S. Grimme, J. Antony, S. Ehrlich, and H. Krieg. A consistent and accurate *ab initio* parametrization of density functional dispersion correction (DFT-D) for the 94 elements H-Pu. *J. Chem. Phys.*, 132(15), 2010.

[25] D. Hajinezhad and M. Hong. Perturbed proximal primal-dual algorithm for nonconvex nonsmooth optimization. *Math. Program.*, 176(1):207–245, 2019.

[26] N. Hallak and M. Teboulle. An adaptive Lagrangian-based scheme for nonconvex composite optimization. *Math. Oper. Res.*, 48(4):2337–2352, 2023.

[27] D. Han. A survey on some recent developments of alternating direction method of multipliers. *J. Oper. Res. Soc. China*, 10(1):1–52, 2022.

[28] W. J. Hehre, R. F. Stewart, and J. A. Pople. Self-consistent molecular-orbital methods. I. Use of Gaussian expansions of Slater-type atomic orbitals. *J. Chem. Phys.*, 51(6):2657–2664, 1969.

[29] M. R. Hestenes. Multiplier and gradient methods. *J. Optim. Theory Appl.*, 4(5):303–320, 1969.

[30] L. T. K. Hien and D. Papadimitriou. An inertial ADMM for a class of nonconvex composite optimization with nonlinear coupling constraints. *J. Global Optim.*, 89(4):927–948, 2024.

[31] P. Hohenberg and W. Kohn. Inhomogeneous electron gas. *Phys. Rev.*, 136(3B):B864, 1964.

[32] J. Hu, X. Liu, Z. Wen, and Y.-X. Yuan. A brief introduction to manifold optimization. *J. Oper. Res. Soc. China*, 8(2):199–248, 2020.

[33] R. D. Johnson III. NIST Computational Chemistry Comparison and Benchmark Database. NIST Standard Reference Database Number 101, 2022.

[34] B. Kaduk, T. Kowalczyk, and T. Van Voorhis. Constrained density functional theory. *Chem. Rev.*, 112(1):321–370, 2012.

[35] W. Kohn and L. J. Sham. Self-consistent equations including exchange and correlation effects. *Phys. Rev.*, 140(4A):A1133, 1965.

[36] W. Kong and R. D. C. Monteiro. An accelerated inexact dampened augmented Lagrangian method for linearly-constrained nonconvex composite optimization problems. *Comput. Optim. Appl.*, 85(2):509–545, 2023.

[37] W. Kong and R. D. C. Monteiro. Global complexity bound of a proximal ADMM for linearly constrained nonseparable nonconvex composite programming. *SIAM J. Optim.*, 34(1):201–224, 2024.

[38] A. Kovnatsky, K. Glashoff, and M. M. Bronstein. MADMM: a generic algorithm for non-smooth optimization on manifolds. In B. Leibe, J. Matas, N. Sebe, and M. Welling, editors, *European Conference on Computer Vision*, volume 9909 of *Lecture Notes in Computer Science*, pages 680–696. Springer, 2016.

[39] G. Kresse and J. Furthmüller. Efficiency of ab-initio total energy calculations for metals and semiconductors using a plane-wave basis set. *Comput. Mater. Sci.*, 6(1):15–50, 1996.

[40] G. Kresse and J. Furthmüller. Efficient iterative schemes for *ab initio* total-energy calculations using a plane-wave basis set. *Phys. Rev. B*, 54(16):11169, 1996.

[41] T. D. Kühne, M. Iannuzzi, M. Del Ben, V. V. Rybkin, P. Seewald, F. Stein, T. Laino, R. Z. Khaliullin, O. Schütt, F. Schiffmann, D. Golze, J. Wilhelm, S. Chulkov, M. H. Bani-Hashemian, V. Weber, U. Borštnik, M. Taillefumier, A. S. Jakobovits, A. Lazzaro, H. Pabst, T. Müller, R. Schade, M. Guidon, S. Andermatt, N. Holmberg, G. K. Schenter, A. Hehn, A. Bussy, F. Belleflamme, G. Tabacchi, A. Glöß, M. Lass, I. Bethune, C. J. Mundy, C. Plessl, M. Watkins, J. VandeVondele, M. Krack, and J. Hutter. CP2K: an electronic structure and molecular dynamics software package - Quickstep: efficient and accurate electronic structure calculations. *J. Chem. Phys.*, 152(19):194103, 2020.

[42] R. Lai and S. Osher. A splitting method for orthogonality constrained problems. *J. Sci. Comput.*, 58(2):431–449, 2014.

[43] J. Li, S. Ma, and T. Srivastava. A Riemannian alternating direction method of multipliers. *Math. Oper. Res.*, 50(4):3222–3242, 2025.

[44] L. Lin, J. Lu, and L. Ying. Numerical methods for Kohn-Sham density functional theory. *Acta Numer.*, 28:405–539, 2019.

[45] X. Liu, X. Wang, Z. Wen, and Y. Yuan. On the convergence of the self-consistent field iteration in Kohn-Sham density functional theory. *SIAM J. Matrix Anal. Appl.*, 35(2):546–558, 2014.

[46] X. Liu, Z. Wen, X. Wang, M. Ulbrich, and Y. Yuan. On the analysis of the discretized Kohn-Sham density functional theory. *SIAM J. Numer. Anal.*, 53(4):1758–1785, 2015.

[47] C. Lu, J. Feng, Z. Lin, and S. Yan. Nonconvex sparse spectral clustering by alternating direction method of multipliers and its convergence analysis. In *Proceedings of the AAAI Conference on Artificial Intelligence*, volume 32, 2018.

[48] P.-W. Ma and S. L. Dudarev. Constrained density functional for noncollinear magnetism. *Phys. Rev. B*, 91(5):054420, 2015.

[49] J. G. Melo, R. D. C. Monteiro, and H. Wang. Iteration-Complexity of an Inexact Proximal Accelerated Augmented Lagrangian Method for Solving Linearly Constrained Smooth Nonconvex Composite Optimization Problems. arXiv preprint arXiv:2006.08048, 2020.

[50] J. P. Perdew, K. Burke, and M. Ernzerhof. Generalized gradient approximation made simple. *Phys. Rev. Lett.*, 77(18):3865–3868, 1996.

[51] M. J. D. Powell. A method for nonlinear constraints in minimization problems. In R. Fletcher, editor, *Optimization*, pages 283–298. Academic Press, 1969.

[52] P. Pulay. Convergence acceleration of iterative sequences. The case of SCF iteration. *Chem. Phys. Lett.*, 73(2):393–398, 1980.

[53] P. Pulay. Improved SCF convergence acceleration. *J. Comput. Chem.*, 3(4):556–560, 1982.

[54] K. Sun and X. A. Sun. Dual descent augmented Lagrangian method and alternating direction method of multipliers. *SIAM J. Optim.*, 34(2):1679–1707, 2024.

[55] Q. Sun, X. Zhang, S. Banerjee, P. Bao, M. Barbry, N. S. Blunt, N. A. Bogdanov, G. H. Booth, J. Chen, Z.-H. Cui, J. J. Eriksen, Y. Gao, S. Guo, J. Hermann, M. R. Hermes, K. Koh, P. Koval, S. Lehtola, Z. Li, J. Liu, N. Mardirossian, J. D. McClain, M. Motta, B. Mussard, H. Q. Pham, A. Pulkin, W. Purwanto, P. J. Robinson, E. Ronca, E. R. Sayfutyarova, M. Scheurer, H. F. Schurkus, J. E. T. Smith, C. Sun, S.-N. Sun, S. Upadhyay, L. K. Wagner, X. Wang, A. White, J. D. Whitfield, M. J. Williamson, S. Wouters, J. Yang, J. M. Yu, T. Zhu, T. C. Berkelbach, S. Sharma, A. Y. Sokolov, and G. K.-L. Chan. Recent developments in the PySCF program package. *J. Chem. Phys.*, 153(2):024109, 2020.

[56] N. J. Turro, V. Ramamurthy, and J. C. Scaiano. *Principles of Molecular Photochemistry: an Introduction*. University Science Books, 2009.

[57] J. H. Van Lenthe, R. Zwaans, H. J. J. Van Dam, and M. F. Guest. Starting SCF calculations by superposition of atomic densities. *J. Comput. Chem.*, 27(8):926–932, 2006.

[58] L. Wang, X. Liu, and Y. Zhang. A communication-efficient and privacy-aware distributed algorithm for sparse PCA. *Comput. Optim. Appl.*, 85(3):1033–1072, 2023.

[59] L. Wang, X. Liu, and Y. Zhang. Seeking consensus on subspaces in federated principal component analysis. *J. Optim. Theory Appl.*, 203(1):529–561, 2024.

[60] F. Weigend and R. Ahlrichs. Balanced basis sets of split valence, triple zeta valence and quadruple zeta valence quality for H to Rn: design and assessment of accuracy. *Phys. Chem. Chem. Phys.*, 7(18):3297–3305, 2005.

[61] Q. Wu and T. Van Voorhis. Direct optimization method to study constrained systems within density-functional theory. *Phys. Rev. A*, 72(2):024502, 2005.

[62] Q. Wu and T. Van Voorhis. Constrained density functional theory and its application in long-range electron transfer. *J. Chem. Theory Comput.*, 2(3):765–774, 2006.

[63] L. Yang, T. K. Pong, and X. Chen. Alternating direction method of multipliers for a class of nonconvex and nonsmooth problems with applications to background/foreground extraction. *SIAM J. Imag. Sci.*, 10(1):74–110, 2017.

[64] H. Yu, B. Liu, Y. Zhong, L. Hong, J. Ji, C. Xu, X. Gong, and H. Xiang. Physics-informed time-reversal equivariant neural network potential for magnetic materials. *Phys. Rev. B*, 110(10):104427, 2024.

[65] H. Yu, Y. Zhong, L. Hong, C. Xu, W. Ren, X. Gong, and H. Xiang. Spin-dependent graph neural network potential for magnetic materials. *Phys. Rev. B*, 109(14):144426, 2024.

[66] J. Zhang, S. Ma, and S. Zhang. Primal-dual optimization algorithms over Riemannian manifolds: an iteration complexity analysis. *Math. Program.*, 184(1):445–490, 2020.

[67] D. Zheng, X. Peng, Y. Huang, Y. Wang, D. Zhang, Z. Huang, Z. Cai, L. Zhang, M. Chen, B. Xu, and W. Zhou. Integrating deep-learning-based magnetic model and non-collinear spin-constrained method: methodology, implementation and application. *npj Comput. Mater.*, 2026.

[68] Y. Zhou, X. Shi, L. Guo, J. Cao, and M. Abdel-Aty. Perturbed Proximal Gradient ADMM for Nonconvex Composite Optimization. arXiv preprint arXiv:2504.12759, 2025.

[69] D. Zhu, L. Zhao, and S. Zhang. A first-order primal-dual method for nonconvex constrained optimization based on the augmented Lagrangian. *Math. Oper. Res.*, 49(1):125–150, 2024.